



NJC

The crystalline state of rubrene materials: intermolecular recognition, isomorphism, polymorphism, and periodic bond-chain analysis of morphologies

Journal:	<i>New Journal of Chemistry</i>
Manuscript ID	NJ-ART-02-2022-000861.R1
Article Type:	Paper
Date Submitted by the Author:	n/a
Complete List of Authors:	Moret, Massimo; Universita degli Studi di Milano-Bicocca, Scienza dei Materiali Gavezzotti, Angelo; Universita di Milano, Dipartimento di Chimica

SCHOLARONE™
Manuscripts

ARTICLE

The crystalline state of rubrene materials: intermolecular recognition, isomorphism, polymorphism, and periodic bond-chain analysis of morphologies†

Received 00th January 20xx,
Accepted 00th January 20xx

Massimo Moret,^{*a} and Angelo Gavezzotti^b

DOI: 10.1039/x0xx00000x

A survey of all crystal structures of rubrene materials in the Cambridge Structural Database is presented. Although the chemical substitution landscape is wide, hydrogen bonding functionalities are absent. Recognition motifs frequently found in crystals are the "slipped-cofacial" molecular pairing, and herringbone or purely translational 3-D propagation. Packing modes are classified in terms of structure determinants, cohesive energies of pairs of molecules in closer contact computed by the CLP atom-atom potential field. In these terms, crystal isomorphism with different chemical substitution is quantitatively assessed. Polymorphs are relatively few, perhaps due to poor solubilities that hamper crystallization screenings. True polymorphs are also identified by structure determinant patterns, and a new polymorph of the di-*p*-nitrophenyl derivative has been prepared and characterized by X-ray diffraction. Crystal morphologies of selected rubrenes have been predicted by Hartman's Periodic Bond Chain approach using PIXEL attachment energies; there is good agreement with experimental morphologies of crystals grown by sublimation. The good results obtained by CLP and PIXEL show promise for a computationally cheap access to lattice energies and morphology prediction. In general, from our overview it looks like sensitive spots in the driving forces for rubrene packing are the 4-substitution sites at the lateral rings, with substituents of moderate steric bulk. Peripheral substitution at the tetracene core seems to be less relevant. Our survey provides a structural background fostering new ideas on the synthesis and planning of physical properties of rubrenes.

Introduction

Organic semiconductors have been for a long time under scrutiny for the development of organic electronic devices.^{1,2} Among a host of molecular candidates, rubrene (5,6,11,12-tetraphenyl-tetracene) has been at the forefront of research after discovery of the high charge-carrier mobility of its orthorhombic polymorph.^{3,4} Although organic semiconductors have not yet reached performance levels suitable for extensive marketing, the synthesis and the characterization of rubrene derivatives are still highly attractive.⁵

A primary issue is the design of high yield chemical synthetic paths, but a better understanding of the solid-state properties of these organic crystals is also desirable because physical properties depend on detail of crystal packing. Intermolecular interactions determine the crystal structure, influencing charge-carrier mobility, transfer integrals and exciton diffusion length.⁶ Bulk charge-

transport properties are related to π -stacking interactions, arising from orbital overlap of adjacent molecules. In the nearest-neighbor stacking arrangement of the rubrene crystal the presence of lateral phenyls forces a slippage on the long molecular axis of the tetracene core, forming a hopping pair called "slipped-cofacial"⁷ with a distance of 3.74 Å, larger than in typical π -stacks^{8,9} and in tetracene itself.⁷ Stacking geometries are also influenced by the twisting of the tetracene core imposed by intramolecular strain. The pair propagates in rows that are the main direction of conduction¹⁰ with a high value of the transfer integrals.¹¹ These rows often pack in a zig-zag fashion, giving the crystal the so-called "herringbone" shape (Fig. 1).

The preparation of effective semiconducting organic materials depends on i) finding molecules with improved solubility and stability against light and/or oxygen degradation¹² (lack of these features is a drawback of pristine rubrene); and ii) obtaining crystal structures with planar polyacene cores and optimum π - π overlap. The task is, to say the least, awkward. In fact, previous analyses of crystal packing in rubrene derivatives (see reference 5 and references therein) focussed on π - π stacking distances, slip distances and angles, tetracene planarity, herringbone angles, trying to find a rationale for enhancement of transport properties through chemical modification. However, a study based on graphical tools found little or no correlation between planarity of the tetracene core and the nature of lateral substituents.¹³

Modification of the rubrene molecule at the rim of the tetracene core frequently results in the disruption of the herringbone motif and/or significant twisting of the tetracene backbone. Partial or

^a Department of Materials Science, University of Milano - Bicocca (Italy)
E-mail massimo.moret@unimib.it

^b Department of Chemistry, University of Milano (retired) (Italy)
E-mail angelo.gavezzotti@unimi.it

†Electronic Supplementary Information (ESI) available: an Appendix on crystallographic terminology, more crystal packing and aggregation diagrams as mentioned in the text; numerical detail of the partitioned Coulombic-dispersion energies and comparison of force fields, energy crystal graphs for PBC modeling of crystal morphologies. Deposition number 2149694 contains single crystal X-ray data of the triclinic polymorph of 5,11-bis(4-nitrophenyl)-6,12-diphenyltetracene (provisionally called here CIYNAB01). These data are provided free of charge by the joint Cambridge Structural Data Centre and Fachinformationszentrum Karlsruhe Access Structure service www.ccdc.cam.ac.uk/structures. See DOI: 10.1039/x0xx00000x

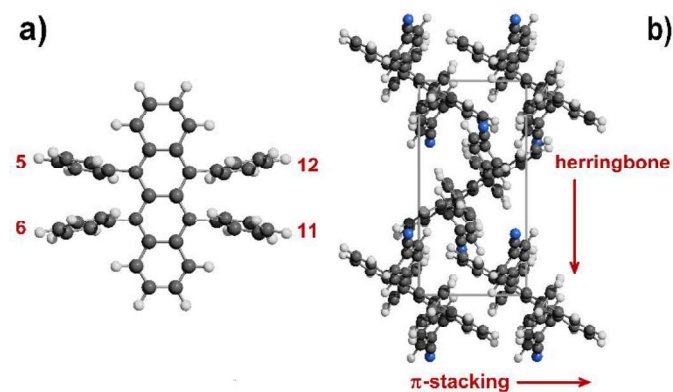


Fig. 1 (a) The rubrene molecule with position numbering of phenyl, thiophene, furan or pyridine rings. (b) Some key structural features in rubrene crystals: π -stacking is in the slipped-cofacial form. Tetracene rings are seen edge-on (example taken from CIYYAM, see Table 1).

complete tetracene fluorination provides a planar tetracene core in only two cases but with loss of the favourable rubrene packing mode.^{14,15} A more promising route involves substitution at the *para* and *meta* positions of the attached phenyl rings, trying to preserve both a planar tetracene core and the (200) slice of orthorhombic rubrene.^{16,17} These new derivatives allowed a characterization of oxygen/light stability and charge transport properties, providing new hints about the relation between molecular architectures, crystal structures and physical properties. With introduction of *para* functional groups on centrosymmetric rings 5 and 11¹⁷ the unmodified tetracene core preserved the structural motif of the (200) monomolecular slice, although the stacking of layers was no longer feasible in the orthorhombic system due to the increased corrugation of the (h00) surface. The strong repulsion caused by crowded peripheral phenyl rings can be reduced by twisting of the tetracene backbone, resulting in a conformation that is the most stable for molecules in solution, vapour phase and amorphous solids.¹⁸⁻²⁰ Tetracene twisting is detrimental to the desired electronic properties; unfortunately, this is observed in about half of the crystalline derivatives, due to a combination of intra- and intermolecular steric factors.

Polymorphism is also an issue. Pristine rubrene has three polymorphs (orthorhombic, monoclinic and triclinic) obtained under ambient conditions by crystallization from different solvents or by vacuum techniques, plus a high-pressure triclinic structure stable above ca. 6 GPa.²¹ The mobility in the orthorhombic polymorph²² is an order of magnitude greater than that of the triclinic polymorph, that has a different propagation pattern and a smaller short-axis displacement.²³ The monoclinic polymorph shows no π -stacking with a corresponding poor performance.²⁴

The main task of organic crystal chemistry is to trace a consequential connection between molecular structure and crystal packing, at least in its essential features if not in a complete crystal structure prediction. Such studies rely on a statistical approach based on crystal and molecular geometries as found in experimental diffraction work, supplemented by a quantitative analysis of packing energies and forces. Previous attempts on various small subsets of functionalized rubrenes tried to extract general trends;^{13,18,25-27} we

present here a survey of molecular and crystal properties of 33 tetra(ring)-substituted tetracenes with rubrene-like architecture, fully characterized by single-crystal X-ray diffraction, along with a detailed analysis of their intermolecular energies and crystal packing modes. In a different perspective to the same aim, the equilibrium and growth morphologies of crystals of orthorhombic rubrene and four monoclinic derivatives¹⁷ have been modeled. Crystal morphology depends mainly on intermolecular potentials that determine anisotropic growth forces, but other external, thermodynamic, and kinetic factors are at work, including supersaturation, temperature, pH, the influence of solvent, of impurities or additives, and the presence of electromagnetic or mechanical fields. The theoretical crystal morphology can be derived solely from the crystal structure by Periodic Bond Chain (PBC) methods,²⁸⁻³⁰ whereby a crystal structure is seen as a 3D array of uninterrupted chains of strong bonds with the crystal's stoichiometry, running along specific crystallographic [uvw] directions. The method works under the assumptions that *i*) crystal growth is controlled by surface processes (incorporation of growth units); *ii*) during crystal growth strong intermolecular bonds are formed between growth units; *iii*) external factors play only a minor role (growth performed at low/moderate supersaturations). Obviously, a reliable method for the quantitative evaluation of the energies of these bonds must be available.

Results and Discussion

Structure screening: a normalized dataset of rubrenes

Table S1 (ESI†) has a list of all the rubrene crystal structures in the Cambridge Structural Database (CSD,³¹ labeled by their six-letter Refcode identifier). A preliminary screening to assess the adaptability of each structure to a systematic crystal packing analysis was carried out, as described below. The main features that guided the selection were a) 5,6,11,12-substitution only by ring compounds, phenyls, furans, pyridines, or thiophenes; b) available unit cell dimensions, space group and atomic coordinates for all non-hydrogen atoms; c) no unresolved disorder; d) *R*-factors below 7.5% (with one exception). Unreliable or absent hydrogen atom positions were corrected or provided by standard procedures in ad hoc modules of the MiCMoS platform (see the documentation at sites.unimi.it/xtal_chem_group/). The MiCMoS module Crysaa was used to make sure that no undetected errors in atom positions, space group assignment, etc., were present. The presently determined structure of a polymorph of CIYNAB, provisionally labeled CIYNAB01, was also considered. Two resolved twins (RAGDEL, VICHAT) were included, and two partially disordered structures (RAGDAH, PIXPUJ01) were included using the major component of disorder. The polymorphs GORVIU, PIXPOD and PIXPUJ, although interesting, could not be included due to major disorder that prevents a unique analysis in our terms. The final dataset of 33 crystal structures (Table 1) can be used with confidence for further theoretical studies. A complete list of atomic coordinates including hydrogen atoms is available from the authors upon request.

Table 1 Molecular and crystal data of rubrenes in the optimized Database. Table S1 (ESI†) has other detail and cell dimensions

Refcode ^[a]	Space group	Z ^[b]	Z' ^[c]	sym ^[d]	twist ^[e]	T / K	Rfac ^[f]	Description of substituents ^[g]
AXIDER	P2 ₁ /c	2	1/2	I	0	293	6.35	5,11(PhF) 6,12(Ph) T(2,8Fluoro) ^[h]
CIYNAB	P2 ₁ /c	2	1/2	I	0	153	6.73	5,11(PhNO ₂) 6,12(Ph)
CIYNAB01	P $\bar{1}$	1	1/2	I	0	293	7.45	5,11(PhNO ₂) 6,12(Ph)
CIYXUF	P2 ₁ /c	2	1/2	I	0	123	6.59	5,11(Ph) 6,12(PhCF ₃)
CIYYAM	P2 ₁ /c	2	1/2	I	0	120	6.65	5,11(PhCN) 6,12(Ph)
GORVIU01	P2 ₁ /c	4	1	-	18	93	4.60	5,6,11,12(Furan)
GORVUG	P $\bar{1}$	2	1	-	18	93	4.50	5,6,11,12(MeFuran)
INELUK	P2 ₁ /n	4	1	-	25	123	5.62	perfluororubrene
INELUK02	P2 ₁ /c	2	1/2	I	0	173	4.50	perfluororubrene
MIVCUR	C2/c	12	3/2	I	0	173	4.75	5,6,11,12(PhMe)
MIVDAY	P2 ₁	2	1	-	18	173	4.31	5,12(PhMe ₂) 6,11(PhMe)
MIVDEC	Pna2 ₁	4	1	-	21	173	4.21	5,12(PhMe) 6,11(Ph)
MIVDOM	Pbcm	4	1/2	M	0	123	7.61	5,12(PhMe) 6,11(PhCF ₃)
MIVDUS	Pnma	4	1/2	M	0	123	4.59	5,12(Ph) 6,11(PhCF ₃)
PIFHIW	Pnma	4	1/2	M	0	292	7.42	5,12(PhtBu) 6,11(Ph)
PIFHOC	P2 ₁ /c	4	1	-	24	292	9.77	5,11-(PhtBu) 6,12(Ph)
PIXPOD01	P2 ₁ /c	4	1	-	20	93	5.01	5,6,11,12(Thiophene)
PIXPUJ01 ^[i]	P2 ₁ /c	2	1/2	I	0	120	6.87	5,11(Thiophene) 6,12(Ph)
POGZIV	P2 ₁ /c	8	2	-	15, 20	294	6.91	5,12(Thiophene) 6,11(Ph)
QQQCIG05	Cmca	4	1/4	I A M	0	125	3.77	5,6,11,12(Ph) rubrene
QQQCIG13	P2 ₁ /c	2	1/2	I	0	173	4.94	5,6,11,12(Ph) rubrene
QQQCIG14	P $\bar{1}$	1	1/2	I	0	173	6.72	5,6,11,12(Ph) rubrene
RAGCEK	P2 ₁ /c	4	1	-	11	123	5.59	5,12(Ph(CF ₃) ₂) 6,11(PhMe)
RAGCIO	P2/c	4	1	-	0	123	6.14	5,12(PhtBu) 6,11(PhCF ₃)
RAGCUA	C2/c	4	1/2	A	13	123	3.74	5,12(Ph) 6,11(C ₆ F ₄ CF ₃)
RAGDAH ^[j]	P2 ₁ /n	4	1	-	16	123	3.23	5,12(PhMe) 6,11(C ₆ F ₄ CF ₃)
RAGDEL	P $\bar{1}$	2	1	-	13	123	4.71	5,12(C ₆ F ₅) 6,11(Ph) ^[j]
RAGDIP	P $\bar{1}$	2	2	-	0	123	3.89	5,6,11,12(C ₆ F ₅)
RAGDOV	C2/c	4	1/2	A	9	123	7.13	5,6,11,12(PhCF ₃)
TEFDUG	Pnna	4	1/2	A	16	173	7.48	5,12(C ₆ F ₅) 6,11(Ph) T(1,2,3,4Fluoro) ^[h]
TOMVOH	Pbca	8	1	-	25	120	4.15	5,12(PhOMe) 6,11(Ph)
TOMWAU	P2 ₁ /n	4	1	-	20	120	5.59	5,12(PhF) 6(Ph) 11(PhOMe)
VICHAT	P $\bar{1}$	1	1/2	I	0	100	4.09	6,12(Ph) 5,11(Pyridine) ^[j]

[a] Identification code of the Cambridge Structural Database (CSD). [b] Molecules in unit cell. [c] Molecules in asymmetric unit. [d] Intramolecular symmetry: I inversion, A twofold axis, M mirror. [e] C-C-C *cis* torsion angle across the central C=C bond in tetracene (*trans* is 180-*cis*). [f] Crystallographic *R*-factor. [g] Ph=phenyl, Me=methyl, t-Bu=tert-butyl, CF₃=trifluoromethyl. In PhX codes, the X substituent is in the *para* position unless otherwise stated. [h] Substitution at the tetracene ring. [i] Major component of disorder. [j] Resolved twin

Force field assessment

The choice of a suitable force field is imperative in the present case and must be made with a careful maximization of the efficiency/cost ratio. The focus being on intermolecular contact, all molecules are kept in the geometry determined by X-rays so that no intramolecular force field is necessary.

Intramolecular energy terms can be neglected when discussing interaction energies between pairs of molecules, that are just tracers of the packing arrangement in the crystal. Intramolecular factors may be important for comparisons between total crystal energies; a procedure for an approximate evaluation will be described for the

case of perfluororubrene (see below). The choice of a suitable intermolecular force field must be made maximizing the efficiency/cost ratio. The MicMoS environment offers three schemes for intermolecular potentials, listed in order of increasing accuracy: a) the AA-CLP formulation,³² an atom-atom scheme of entirely empirical origin, that requires only a few seconds; b) the AA-LJC formulation,³³ also atom-atom but requiring atomic point-charge parameters derived from an MP2-MO wavefunction; the molecular orbital calculation is demanding for the big rubrenes, but lattice energy calculations take fractions of a second; c) the PIXEL scheme,³⁴ that requires an MP2-level electron density and also a considerable

amount of computing time for lattice calculations by finite integration of the various operators on the discrete wavefunction. The three methods work with default library parameters for organic compounds, and provide separate Coulomb, dispersion, and repulsion terms (CLP and Pixel also include a polarization term). Table S2 (ESI[†]) shows that the three approaches provide the same energy trends and often quite similar absolute energy values. Therefore, in large scale structure comparisons the cheapest CLP method was applied, while the accurate Pixel method was used in the analysis of periodic bond chains for some representative compounds. Table S3 (ESI[†]) collects the detail of partitioned lattice energies for all crystals in Table 1.

Crystallography of rubrenes: General aspects

The sample is too small for statistics on space group frequency, but the obvious $P2_1/c$ is predominant. Depending on molecular constitution, rubrene molecules can have internal inversion, mirror or twofold axis symmetry preserved in the crystal, with 1/4, 1/2, 1, 3/2 or 2 molecules in the asymmetric unit. Although the shape of the basic packer is so irregular, packing coefficients

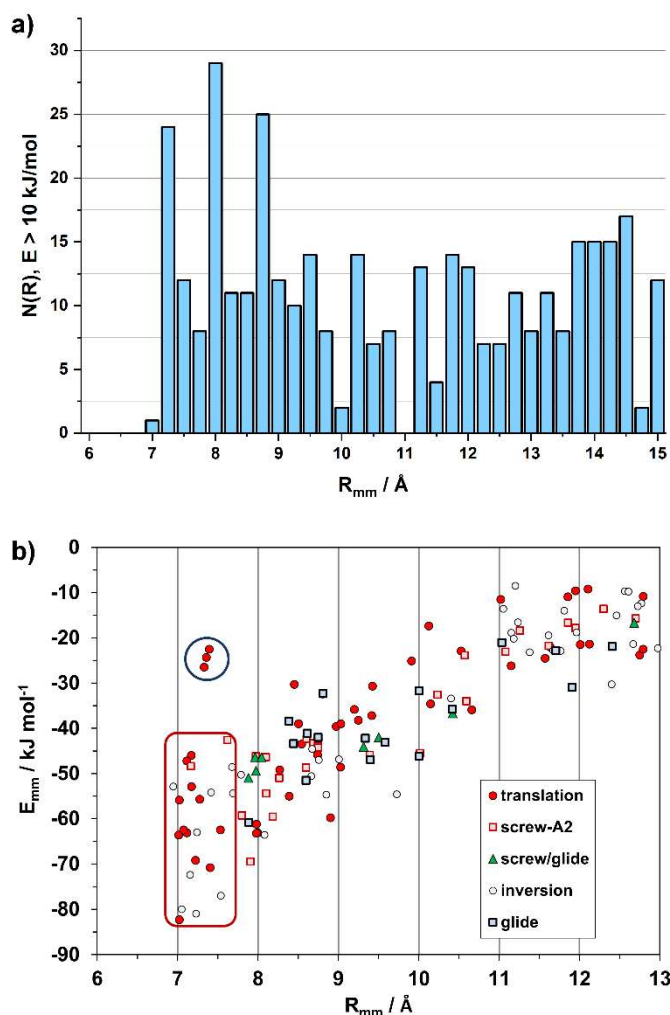


Fig. 2 (a) Histogram of 436 distances between pairs of molecules (R_{mm}) whose stabilization energy is $> 10 \text{ kJ mol}^{-1}$. (b) Energy/distance plot for the independent pairs with labeling of the symmetry operations, O_{mm} . The red rectangle encloses the short distance, inversion-translation domain. See Fig. S1 (ESI[†]) for the outliers in the upper left part (blue circle, and Fig. S2 for the subset of slipped-cofacial.

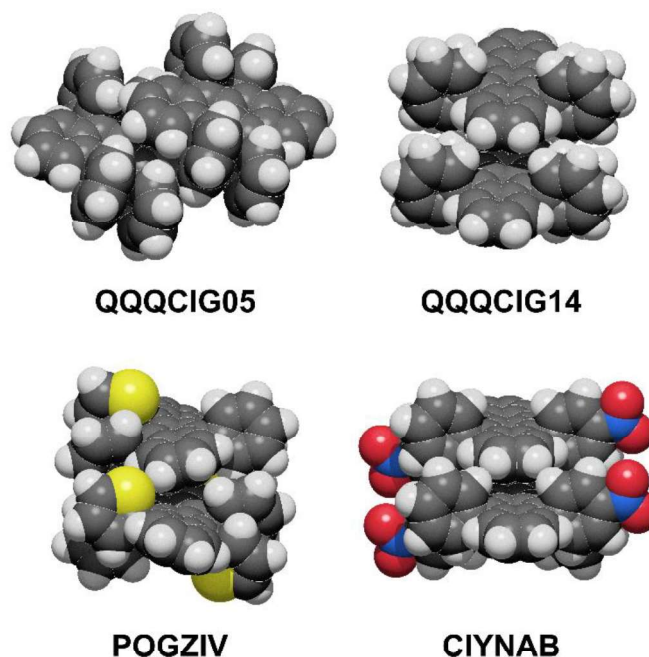


Fig. 3 The slipped-cofacial arrangement: top, in two polymorphs of the parent compound; below: POGZIV shows a twisted tetracene core. Oxygen red, nitrogen blue, sulfur yellow.

are normal (0.68 to 0.74), and nearly all crystal structures show a 10-12-first-neighbor coordination sphere resembling a close packing of spheroids. There are no short atom-atom distances below the sum of contact radii, leaving no ground for the introduction of intermolecular "bonds". Rubrene lattice energies are dominated by dispersive factors (Table S3, ESI[†]), because carbon and hydrogen atoms account for 91% of the total in the database, fluorine contributing another 7%, so that no "polar" groups are present. There are no hydrogen bond donors in our database, preventing a test of competition between dispersion and hydrogen bonding.

Structure determinants and pairing symmetries

Intermolecular structure can be conveniently analyzed by partitioning the total lattice sums into interaction energies between pairs of molecules (E_{mm}). While the lattice energy is comparable to sublimation heats, the E_{mm} 's are purely computational quantities, having no experimental counterpart. The E_{mm} , the corresponding distance R_{mm} between molecular centers of coordinates, and the symmetry operator acting between the two partners, O_{mm} , form a triad called a structure determinant. These determinants are of great help in a quantitative description and comparison of packing modes. In a way, they are zero-dimensional precursors of the periodic bond chains.

Fig. 2a shows a histogram of the R_{mm} distribution, with peaks at the 7.0-7.25 and 7.75-8.0 Å bins. In fact, 21 out of 33 crystals show R_{mm} 's of 7-8 Å either by translation (cell axis length) or by some other symmetry or asymmetry relationship. Fig. 2b shows the distribution of structure determinants. The plot has an obvious bias to higher E_{mm} for shorter R_{mm} , meeting a lower limit at 7 Å. With few exceptions, translation and inversion are the only symmetries that allow a pairing below 8 Å and an energy in excess of 50 kJ mol^{-1} . There is a dip in

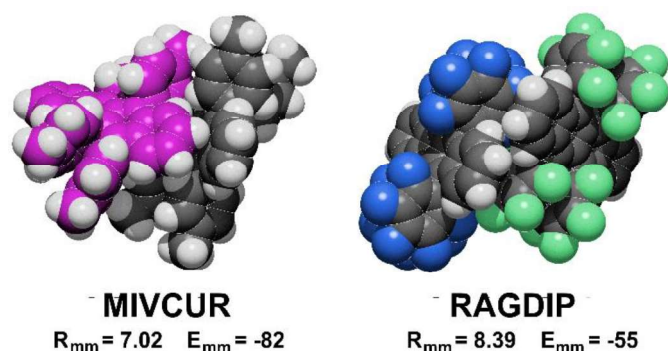


Fig. 4 Examples of coupling modes between pairs in the asymmetric unit. Left: carbon atoms of one molecule magenta; right: fluorine atoms blue in one molecule, green in the other (R_{mm} Å, E_{mm} kJ mol⁻¹).

frequency between 9.5 and 11 Å, while the distribution levels at 10–25 kJ mol⁻¹ with distances > 10 Å at second-neighbor stage, as recognition becomes less selective.

The most common coupling mode at short intermolecular distance is called "slipped-cofacial", a parallel arrangement of the tetracenes allowing as much π -overlap as possible compatibly with the clash at the interlocking of lateral ring substituents. Fig. 3 shows some examples of these dimer structures, while Fig. S3 (ESI[†]) has an extended gallery of such coupling patterns. This mode occurs with $7 < R_{mm} < 8$ Å, being called the SC7 mode. Fig. S2 (ESI[†]) and Table S4 (ESI[†]) show that there is no correlation between distance and energy because much depends also on the nature of the lateral substituents.

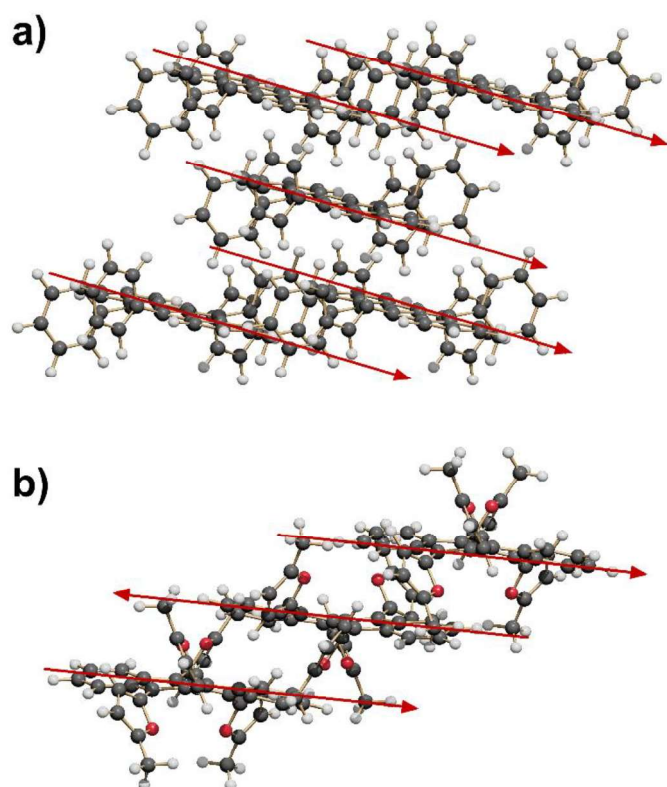


Fig. 5 $P\bar{1}$ space groups. (a) Expansion of the SC7 motif by coordination into a fourfold cage of translation related molecules (QQCIG14). (b) Propagation into ribbons of alternate inversion-related molecules (GORVUG).

This configuration is fostered almost exclusively by dispersion, although some charge-transfer contribution may be also present.

A definite symmetry relationship is not a prerequisite for short distance stabilization. The most stable pair in the database, -82 kJ mol⁻¹, is the asymmetric pair in MIVCUR (Fig. 4). An example of infrequent short distance coupling over a screw axis is MIVDOM (Fig. S4, ESI[†]) with an E_{mm} of -70 kJ mol⁻¹ between non-parallel tetracene units. In a few cases, 7 Å couplings with low stabilization result from parallel tetracene cores without offset (Fig. S1, ESI[†]).

Coordination spheres and extended packing motifs

Since the reciprocal orientation of tetracene planes is so important for the physical properties of rubrenes, this feature is now taken as the leading one in the analysis of extended crystal packing. In the six $P\bar{1}$ space groups, and in two $C2/c$, $Z' = 1/2$ space groups with the tetracene plane riding a twofold axis (see Table 1), any symmetry operation (translation, inversion and centering) can only produce a parallel alignment of tetracenes. The slipped-cofacial motif at 7 Å distance ("SC7" motif) is expanded by pure translation (Fig. 5a) or by inversion (Fig. 5b).

In other $Z' = 1$ structures with screw and/or glide operations the 3D expansion produces a corrugated arrangement of tetracenes. A

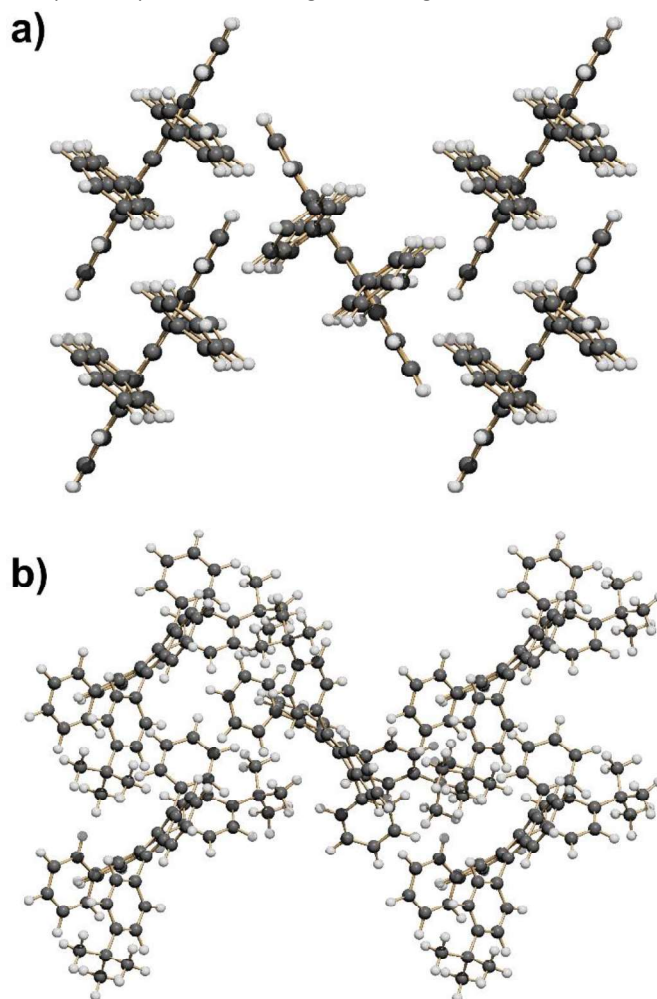


Fig. 6 (a) The SC7 + 4 Screw herringbone-cage mode here exemplified by QQCIG05 (compare with Fig. 1b). (b) The T9 + 4 Screw herringbone-cage mode here exemplified by PIFHOC.

classification of the structure expansion motifs includes the symmetry operators acting among nearest-neighbor molecules, while a measure of the corrugation is provided by the angles between vectors perpendicular to the average tetracene plane. Fig. S5 and Table S5 (ESI[†]) carry the detail of the classification. A first group includes 8 strictly similar structures with SC7 motif, an interplanar angle close to 60° and a fourfold cage provided by screw operators, as exemplified in Fig. 6a. A second group includes 7 structures whose motif is again a fourfold cage, but with 9 Å translation (Fig. 6b), and a less compact aggregation with a spread of interplanar angles. The aggregation motif in these two groups can be classified as fourfold "herringbone-cage". Six other structures and the three structures with $Z' > 1$ show packing motifs with a complex admixture of first neighbors over various symmetry elements that defies a simple classification.

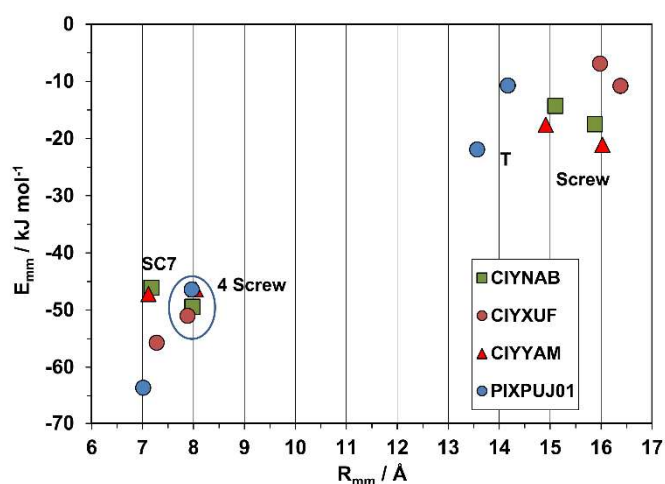


Fig. 7 Energetic profiles (kJ mol^{-1}) for a series of strictly isostructural crystals (see Table 1). SC7 = slipped-cofacial with 7 Å translation; 4 screw, coordination by 4 screw related molecules. The upper right part is manifold of closely related symmetries.

Isostructurality of rubrene crystals

The purely geometrical, qualitative analysis of packing modes can be supplemented by a quantitative analysis of coordination spheres by structure determinants, plotting molecule-molecule energies E_{mm} against distance R_{mm} . These plots constitute a unique energetic profile of a crystal structure, by which similarities and differences can be better appreciated.³⁵

An exemplary case of isostructurality is seen in Fig. 7: four structures with same space group and nearly identical cell parameters (they are also isomorphous). All structures show the SC7 π -stacking pair, but being chemically different, the interaction energy varies from 45-55 kJ mol^{-1} in the three phenyl substituted compounds to 62 kJ mol^{-1} in the thiophene derivative, stabilized by a larger Coulombic contribution. These considerations show that geometrical isomorphism is not always equivalent to energetic isostructurality. The SC7 mode is supplemented by a screw related pairing in the fourfold cage, of nearly identical stabilization in all four structures. The second coordination shell (upper right part of the plot) includes an admixture of screw and translation (T) determinants, in a common area although with minor energetic differences.

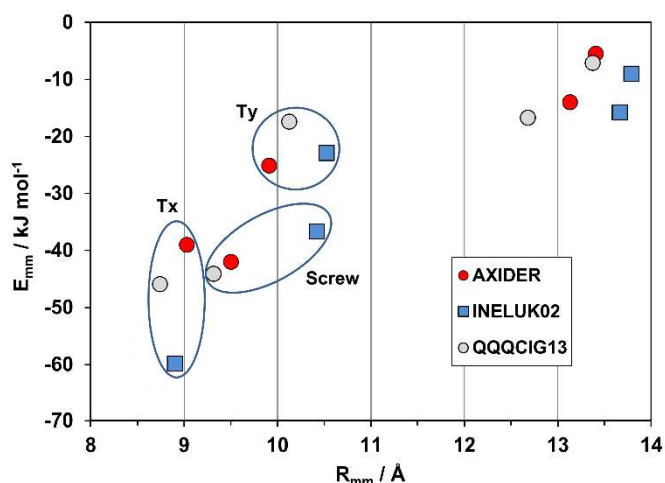


Fig. 8 Energetic profiles (kJ mol^{-1}) for a series of almost isostructural crystals (see Table 1). Tx, Ty: translation along cell edges.

A second very nearly isostructural series is shown in Fig. 8. The compounds are a hydrocarbon (QQQCIG13), a sparsely fluorinated compound (AXIDER) and a perfluoro derivative (INELUK02). The crystal structures are similar (same space group and cell parameters) but the energetic profile of the perfluoro compound shows a much larger cohesive energy in the first determinant, due to a substantial Coulombic contribution (nearly zero in the other two structures). The second determinant is over a longer screw axis relationship, testifying a significant structure deformation due to perfluorination.

The triclinic structures of the parent hydrocarbon (QQQCIG14), of the newly determined polymorph CIYNAB01, and (strangely enough) of the compound in which two lateral phenyls are substituted by pyridines, are isomorphous (same cell parameters). The energy profiles in Fig. 9 prove that they are also isostructural, with a strict correspondence of the first two major determinants. The spread and minor differences in the second-neighbor coordination shell are marginally significant because the interaction energies are anyway small.

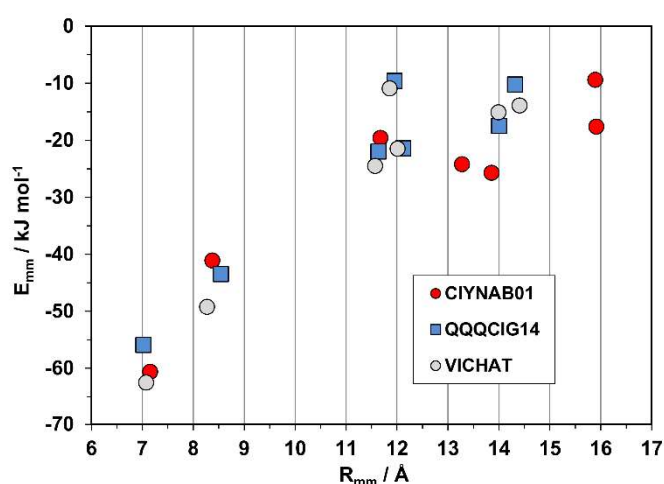


Fig. 9 Energetic profiles (kJ mol^{-1}) for a series of three isostructural triclinic crystals. All pairings are by pure translation.

Polymorphism of rubrenes

The parent compound (database refcode QQQCIG, see Table 1) has three well described polymorphs, and our database includes two other cases of clear cut polymorphism (CIYNAB, INELUK). Other compounds (GORVIU, PIXPOD, PIXPUJ, CIYXUF) are apparently polymorphic, but one of the partners is heavily disordered; in such cases one may wonder whether the postulated polymorphism is a real material property or is rather the result of poor sample quality or handling. In any case these latter instances cannot be adapted to lattice energy analysis and were not considered.

Polymorphism can be discussed qualitatively by comparisons of space groups and cell dimensions, or by packing diagrams, but such analyses are often ambiguous and always suffer from a certain amount of subjectivity. Especially in this case, the energetic profiles offer a univocal quantitative description of structure similarity or differences.

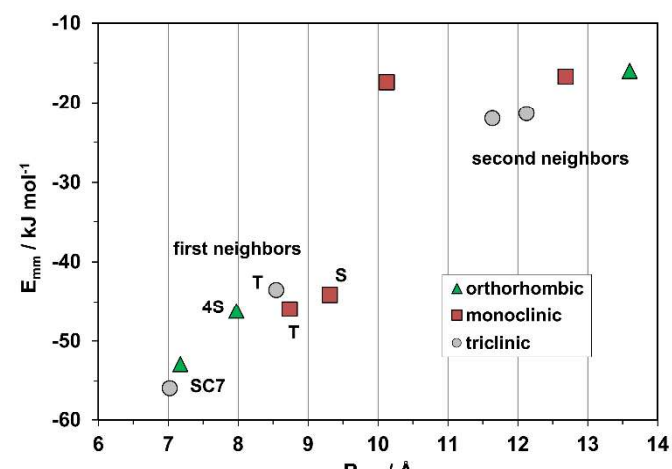


Fig. 10 The energetic profile (kJ mol^{-1}) of the three polymorphs of pristine rubrene, quantifying the different packings.

Fig. 10 shows the profiles for the three polymorphs of the parent hydrocarbon. The stable orthorhombic polymorph and the triclinic polymorph have the same slipped-cofacial pairing by 7 \AA translation (SC7), but then all other determinants are completely different: in particular, the monoclinic polymorph with shortest contact distance of 8.7 \AA stands out as clearly distinct from the other forms. The second neighbor coordination sphere is also quite different in the three structures. These polymorphs are then three clearly distinct material phases, even though they have nearly identical densities and packing coefficients. The AA-CLP lattice energies (207, 205 and 196 kJ mol^{-1} for monoclinic, orthorhombic and triclinic, respectively) are only marginally different, as is very often the case in polymorphic groups. The tetracene core is flat in all polymorphs so that intramolecular energy differences may not be too large. Total energy differences between polymorphs should then be quite small, in agreement with the findings of quantum chemical calculations³⁶ ($\approx 2 \text{ kJ mol}^{-1}$).

Table 2 shows the energy profiles for two polymorphs that crystallize in the same space group but with quite different packing patterns. The polymorph with one full molecule in the asymmetric unit relies mostly on inversion-related neighbors, while the polymorph in which the molecule sits on a crystallographic inversion

center ($Z' = 1/2$) has translation and a fourfold of screw-related molecules in its coordination shell; determinant analysis gives a precise indication of the packing differences. INELUK was determined at lower temperature ($123 \text{ vs. } 173 \text{ K}$) but has nevertheless a lower density ($1.93 \text{ vs. } 2.04 \text{ g cm}^{-3}$) and a lower packing coefficient ($0.72 \text{ vs. } 0.77$): as expected, its total intermolecular energy is much less stabilizing, mainly due to a large deficiency in dispersion (close packing) terms. The tetracene core is flat in INELUK02 but twisted in INELUK, leading to a different overall conformation of the substituents. The non-bonded contact energy between pairs of lateral overlapping C_6F_5 groups, evaluated by the AA-CLP potentials, is destabilizing by 8 kJ mol^{-1} in INELUK02, but stabilizing by 4 kJ mol^{-1} in INELUK: our numbers are a clear indication of tradeoff between favorable intermolecular contact and a less favorable intramolecular conformation. Absolute values may not be good enough for a reliable estimate of the relative stability of the two polymorphs, for which a quantum chemical study³⁶ predicted total energy differences of a few kJ mol^{-1} . Although *R*-factors are comparable ($4.5 \text{ vs. } 5.6\%$), the unusually large lattice energy difference, together with the differences in densities and packing coefficients, suggest that INELUK is a metastable polymorph.

Table 2 Energetic profiles of two polymorphs, INELUK ($P2_1/n$, $Z=4$) and INELUK02 ($P2_1/c$, $Z=2$) Each row is a structure determinant composed of a symmetry operator, a distance between centers of mass and a pairing energy with its Coulombic, polarization, dispersion, and repulsion components. S, Screw, T, translation, INV, inversion center

INELUK $P2_1/n$ $Z=4$						
O_{mm}	R_{mm}	Coul	pol	disp	rep	E_{mm}
INV	8.081	-13.5	-7.2	-73.0	30.1	-63.6
INV	8.663	-8.3	-6.2	-57.9	21.8	-50.6
2S	10.593	-5.7	-5.3	-48.0	25.0	-34.0
2Ty	11.149	-6.7	-3.6	-28.9	13.1	-26.2
2S	11.618	-4.5	-4.3	-35.4	22.3	-21.8
E_{latt}		-34.6	-35.4	-229.3	115.1	-184.2

INELUK02 $P2_1/c$ $Z=2$						
	R_{mm}	Coul	pol	disp	rep	E_{mm}
2T	8.902	-20.4	-6.3	-64.4	31.4	-59.8
4S	10.423	-8.1	-5.3	-48.3	25.0	-36.7
2T	10.527	-0.5	-4.0	-32.0	13.6	-22.9
4S	13.665	-3.5	-3.3	-24.9	15.9	-15.8
E_{latt}		-47.5	-38.6	-262.4	133.4	-215.1

Fig. 11 shows the profiles for the CIYNAB and CIYNAB01 polymorph pair. Densities and packing coefficients of the two polymorphs are identical within a fraction of a percent, and lattice energies within 1 kJ mol^{-1} , but the energy profiles are quite different, proving that CIYNAB01 is a legitimate new polymorphic material.

Periodic bond chains analysis of crystal morphologies

PBC theory^{37,38} has been long exploited for modeling theoretical crystal morphologies. Comparison with experimental outcomes provides useful information about the mechanism of growth processes at the crystal/environment interface.³⁹ The PBC approach best works for growth at low supersaturation, without strong solute-solvent interactions (e.g. vacuum sublimation), and when

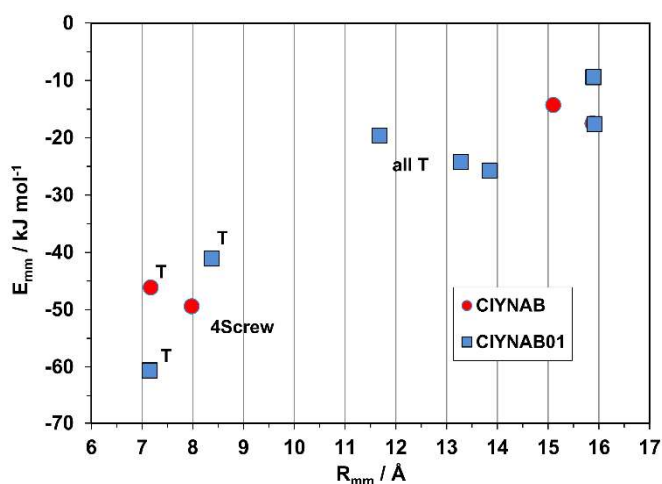


Fig. 11 Proof of the different packing of the new polymorph CIYNAB01.

intermolecular interactions in the growing crystal are dominated by fast decaying dispersive forces³⁹⁻⁴² as the case of rubrenes. The underlying theory assumes that the time needed for the formation of a crystal bond decreases with increasing bond energy, leading to the kinetic equation $R^{hkl} \propto E_{att}^{hkl}$ for flat (F) faces, where R^{hkl} is the growth rate of the (hkl) face and E_{att}^{hkl} is the energy released per growth unit when a slice of d_{hkl} thickness is attached to the surface.³⁸ Therefore, the boundaries of crystal polyhedra are slowly growing faces, mainly flat (F) faces whose attachment energies are usually smaller than those of stepped or kinked faces.^{37,40}

We analyze here in these aspects a set of structures, the orthorhombic parent rubrene (QQQCIG15) and the isomorphous monoclinic derivatives (CIYNAB, CIYXUF, CIYYAM, PIXPUJ01, see Table 1). The growth morphologies of these crystals have been evaluated according to PBC methods^{28,29,40} using intermolecular interactions (called bonds) between first neighbors, whose energy is given by E_{mm} values, derived from the more accurate force field formulation of the PIXEL approach, calculated between a reference molecule and the surrounding molecules within a cutoff of 25 Å. Bonds whose E_{mm} was less than $kT \approx 4 \text{ kJ mol}^{-1}$ (at the actual crystal growth temperature of 500-550 K) were discarded, leaving just four relevant bonds in the selected crystal structures.

The PBC analysis allows to identify crystal planes representing F faces, characterized by two or more non collinear periodic chains running parallel to the pertinent (hkl) plane. Slices of d_{hkl} thickness agreeing with extinction rules of the space group⁴² represent physically sound molecular profiles of surfaces and natural growth layers. The growth units were defined as single molecules with a planar tetracene backbone as observed in the crystal structures. Attachment energies E_{att}^{hkl} for F faces were calculated with the reference molecule interacting with a half crystal exposing the (hkl) plane, applying a 25 Å cutoff for distance between molecular centroids. They were corrected for the energy required to convert the tetracene backbone from the twisted conformation of vapor or solution to the planar one found in crystals, assuming an average value of 10 kJ mol^{-1} from the 6-16 kJ mol^{-1} range.^{18,20,36,43}

Surface energies per unit area $\gamma_{hkl} = W_{hkl} / 2A_{hkl}$ were estimated for a reference molecule attached to the (hkl) plane, where W_{hkl} is the separation work required to split an infinite crystal along the (hkl)

plane and A_{hkl} is the 2D unit cell area. W_{hkl} has been estimated with the same E_{mm} values used for attachment energies, with just minor approximation thanks to the fast decay of intermolecular (mainly dispersion) energies with distance. No significant reconstruction/relaxation has been observed in rubrene surfaces,⁴⁴ supporting the application of Born-Stern definition with cuts of the bulk crystal structure. Theoretical equilibrium and growth crystal morphologies have been obtained with Wulff plots⁴⁵ of γ_{hkl} and E_{att}^{hkl} , respectively.

Table 3 Intermolecular bonds in orthorhombic parent rubrene and flat faces, with bond contributions to slice energy. Sections of the energy crystal graph are reported in Fig. S6 (ESI+).

Bond ^[a]	Symm. op. ^[b]	Distance	Bond energy
a	(x, 1 + y, z)	7.173	-64.8
b	(-x, 1/2-y, 1/2+z)	7.975	-45.9
c	(1/2+x, 1/2+y, z)	13.866	-17.8
d	(1/2-x, -y, 1/2+z)	15.171	-6.5

Flat face	Bonds in slice ^c	E_{att} ^d	γ_{hkl} ^e
{200}	a + 2b	-39.7	80.8
{002}	a + 2c	-94.8	90.6
{111}	b + c + d	-120.6	98.7
{202}	a + d	-121.3	100.2
{020}	2d	-174.2	80.1

[a] Bond between the reference and a neighbor molecule. [b] Symmetry operation connecting reference and neighbor at the listed distance between centers of mass. [c] A slice is a set of layers with overall thickness d_{hkl} . [d] Attachment energy corrected for twisted to flat tetracene backbone. [e] Surface energy, erg cm^{-2} . Distances in Å, energies in kJ mol^{-1} .

Table 3 lists molecule-molecule energies E_{mm} defining bonds for orthorhombic rubrene. Crystal graphs of intermolecular bonds are reported in Fig. S6 (ESI+). The two strongest bonds **a** and **b** lie in the (200) slice and generate a robust growth layer with the slipped-cofacial motif. Within this slice the growth units are incorporated at the end of bond chains, resulting in layer-by-layer growth with stable and flat surface profiles. Experimental evidence from AFM imaging of rubrene {100} surfaces shows accordingly monomolecular (200) steps.⁴⁶⁻⁴⁸ The attachment energy of the {002} surface is more than twice that of {200}, due to the lower energy of the **c** bond. Flat faces {111} and {202} are further down the ranking of E_{att}^{hkl} due to the presence of weaker **d** bonds. Interestingly, the {202} surfaces is similar to a stepped surface with [010] rows (the direction of the strongest bond and PBC) delimited by {200} and {002} facets connected through weak **d** bonds (Fig. S6, ESI+). This face does not appear in the theoretical growth morphology. Similarly, the high E_{att}^{hkl} of face {020}, based only on **d** bonds, makes it disappear from the growth morphology while it is important in the equilibrium shape.

In summary, equilibrium, and even more strongly, growth morphology of orthorhombic rubrene is dominated by {200} surfaces characterized by the lowest E_{att}^{hkl} and γ_{hkl} values (Fig. 12). As reported

for other organic semiconductors⁴⁰⁻⁴² the growth habit is in general less rich in crystal faces than the equilibrium one and displays a higher anisotropy, definitely tabular, determined by the robust slice containing the slipped-cofacial motif. On the contrary, all faces show similar γ_{hkl} , resulting in more isotropic equilibrium crystal habits.

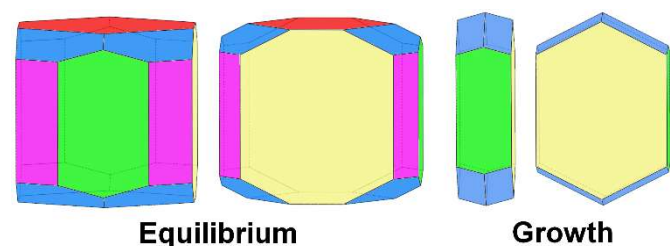


Fig. 12 Equilibrium (left) and growth (right) crystal morphologies of orthorhombic rubrene as predicted by PBC analysis. Color coding: {100} - yellow, {010} - red (absent in growth shape), {001} - green, {101} - violet (absent in growth shape), {111} - blue.

The four monoclinic rubrene derivatives are isomorphous despite different functional groups on rings 5/11 or the presence of thienyl instead of phenyl rings (Table 1). Table 4 shows the results of PBC analysis. All these structures display {100} slices with the slipped-cofacial motif found in the {200} slice of orthorhombic rubrene and share the same four strong bonds. These generate six PBCs ($\{100\}$, $\{010\}$, $\{001\}$, $\langle 011 \rangle$, $\langle 201 \rangle$ and $\langle 211 \rangle$) and five flat faces: $\{100\}$, $\{10\bar{2}\}$, $\{011\}$, $\{002\}$ and $\{11\bar{1}\}$. An example of the crystal graph shared by all structures is reported in Fig. S7 (ESI[†]) for derivative CIYNAB.

Table 4 Intermolecular bonds for isomorphous monoclinic rubrenes (see Table 1 for refcodes) and corresponding flat faces. See Table 3 for units and the meaning of symbols. Surface energies are reported in Table S6 (ESI[†]).

		CIYNAB	CIYXUF	CIYYAM	PIXPUJ01
Bond	Symm. op.	Bond energy			
a	(x, 1+y, z)	-56.8	-57.4	-56.3	-66.0
b	(-x, 1/2+y, 1/2-z)	-50.3	-51.5	-47.2	-39.5
c	(1-x, 1/2+y, 1/2-z)	-23.0	-12.6	-21.4	-11.7
d	(1+x, y, z)	-17.6	-6.1	-20.4	-24.7
Flat face	Bonds in slice	Attachment energy			
{100}	a + 2b	-53.1	-23.4	-55.0	-42.2
{10 $\bar{2}$ }	a + 2c	-105.0	-99.8	-105.5	-94.3
{011}	a + d	-113.5	-108.1	-112.2	-107.9
{002}	b + c + d	-130.6	-114.6	-122.0	-91.3
{11 $\bar{1}$ }	b + c	-131.4	-114.8	-128.0	-128.6
lattice energy		-225.5	-199.6	-218.6	-203.9

Bonds **a** and **b** are in all aspects analogous to orthorhombic rubrene giving rise to the most stable (h00) slice (of d_{100} thickness in the monoclinic structures). The (h00) slice energies are in the range -150/-160 kJ mol⁻¹ out of a lattice energy of -200/-225 kJ mol⁻¹. Bonds **c** and **d** arise from molecular pairs different from those in

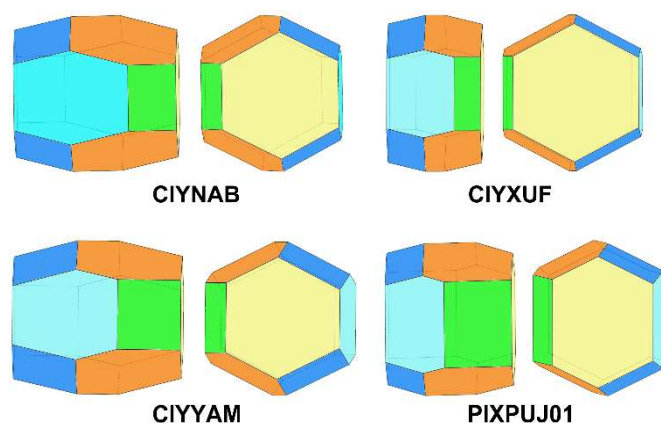


Fig. 13 Equilibrium crystal morphology of isomorphous monoclinic rubrene derivatives CIYNAB, CIYXUF, CIYYAM, PIXPUJ01 as predicted by PBC analysis. Color coding: {100} - yellow, {10 $\bar{2}$ } - cyan, {011} - orange, {001} - green, {11 $\bar{1}$ } - blue.

orthorhombic rubrene because the monoclinic structure allows to accommodate the rougher (h00) interface of protruding *para* substituents (CIYNAB, CIYXUF, CIYYAM) or smaller thienyl rings (PIXPUJ01).

The reduced cohesion in the crystal of fluorinated derivative CIYXUF, with weaker bonds and smaller lattice energy, can be ascribed to the well-known, scarce propensity of hard fluorine for intermolecular stabilization, in contrast with some literature claims of the contrary.

The overall picture of intermolecular interactions is summarized in the theoretical equilibrium and growth morphologies. The decreased surface energy for {100} in the trifluoromethyl derivative produces thinner crystals along the reciprocal direction a^* with an increased morphological relevance of the {100} form (Fig. 13). This effect is more evident in the growth morphologies (Fig. 14) with a tabular habit on {100}, the clearer example being the trifluoromethyl case. Another feature common to these monoclinic crystals is the absence of the {11 $\bar{1}$ } form in the growth shape while {001} is

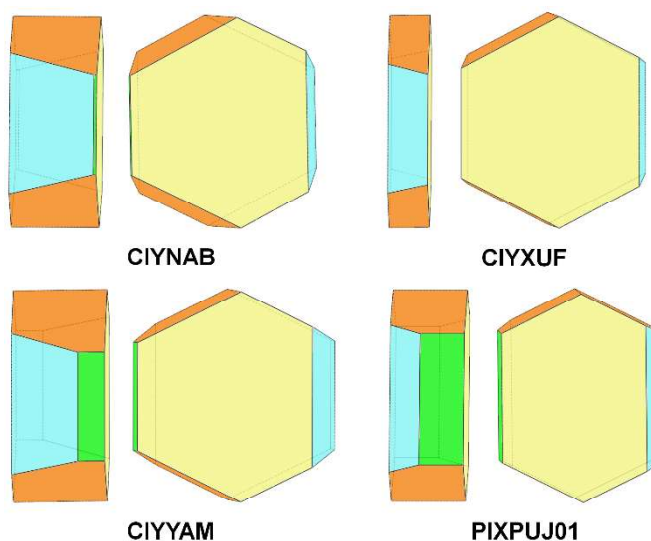


Fig. 14 Growth crystal morphology of isomorphous monoclinic rubrene derivatives CIYNAB, CIYXUF, CIYYAM, PIXPUJ01 as predicted by PBC analysis. Color coding: {100} - yellow, {10 $\bar{2}$ } - cyan, {011} - orange, {001} - green, {11 $\bar{1}$ } absent.

negligible in the nitro-rubrene (CIYNAB) and absent in the trifluoromethyl-rubrene (CIYXUF).

Comparison among predicted and experimental growth crystal morphologies of rubrene derivatives grown in a moderate vacuum can be appreciated in Fig. 15. Further examples of vacuum grown crystals of rubrene are available in several papers.^{48,49} For rubrene and derivatives CIYNAB, CIYXUF and CIYYAM agreement among PBC morphology and experimental ones is satisfactory, considering that significant variability in crystal shapes even under the same experimental conditions is always observed. The strong effect of the trifluoromethyl groups in CIYXUF previously highlighted is clearly demonstrated by the growth of thin tabular crystals (Fig. 15c).

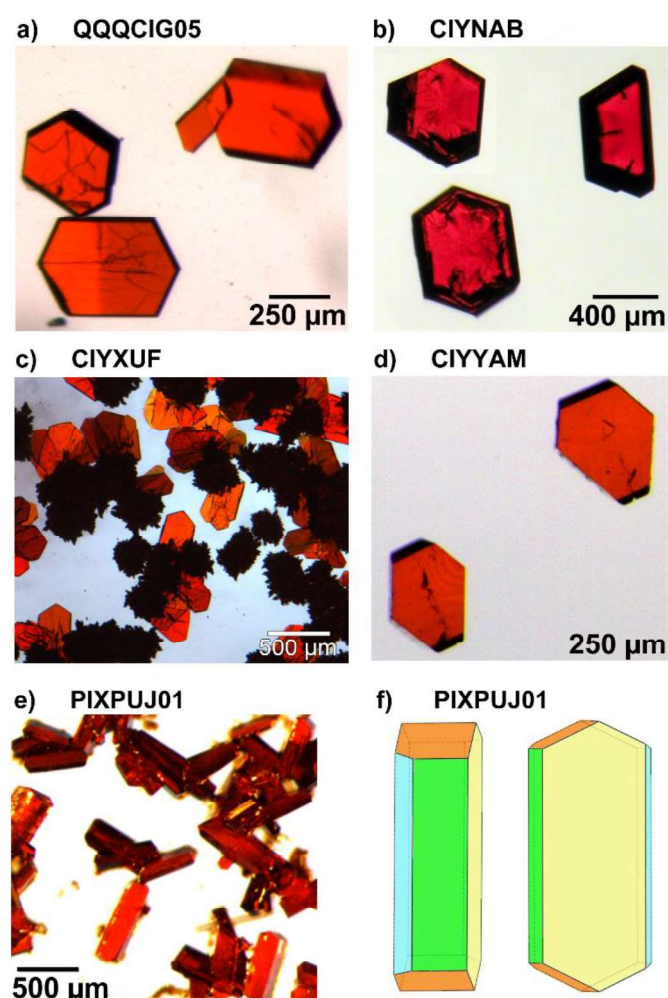


Fig. 15 a-d) Experimental morphologies for crystals of rubrene derivatives grown by vacuum sublimation. In e) are shown crystals of the thienyl derivative grown from hexane/ethyl acetate 9:1 vol/vol. f) sketch of the observed crystal morphology in e) using the color coding of Fig. 14. Crystalline needles shown in c) belong to a concomitant triclinic polymorph.⁵⁰

The thienyl-rubrene PIXPUJ01 could not be vacuum crystallized due to its thermal instability. Crystallization from hexane/ethyl acetate 9:1 vol/vol leads to $[010]$ elongated crystals with $\{100\}$, $\{10\bar{2}\}$ and $\{011\}$ bounding faces. The influence of the solvent mixture and of several byproducts in the final reaction mixture¹⁷ acting as impurities are likely responsible for the modification of the crystal morphology. It is worth mentioning that the monoclinic polymorph

of di-p-nitrophenylrubrene CIYNAB has been obtained also by very slow isothermal evaporation of an acetone solution with a morphology indistinguishable from that of Fig. 15b. Faster isothermal evaporation of an acetone solutions of di-p-nitrophenylrubrene afforded a solvated species.⁵⁰ Examples of the effect of solvent nature upon crystal morphology of pristine rubrene can be found in previous work.^{51,52}

Summary and final remarks

The available crystallography of rubrene materials has been thoroughly reviewed through deposited X-ray determinations, with the aim of establishing a database of fully reliable crystal structures for theoretical studies. The final result was 33 crystal structures double-checked and normalized with respect to hydrogen-atom positions. All the structures include at least one highly stabilizing molecular pair at a center-of-mass distance of 7-8 Å. The database has been analyzed systematically in terms of structural patterns, with a statistical assessment of the frequency of the main aggregation modes. The slipped-cofacial pairing arrangement is almost ubiquitous, being an obvious coupling ("encroaching") mode given the irregular molecular shape: this mode permits as much tetracene stacking as possible, indispensable for promoting transport. Its propagation in three-dimensional monoclinic networks often goes through the herringbone pattern, of which two variants have been found, one with shortest translation of 7 Å and tetracene inter-planar angle of 60°, and another with shortest translation of 9 Å and highly variable inter-planar angles. Triclinic structures occur with a perforce parallel arrangement of tetracene cores. These common features are not exclusive, as examples of other close pairing and propagation modes have been found. Somewhat unexpectedly, in a few cases even asymmetric pairing of two molecules in $Z' = 2$ crystals leads to very high stabilization without intervention of a symmetry operation. Systematization has proceeded to a point, but only sparse clues have appeared as concerns the dependence of packing modes on substituent chemistry, or on molecular conformation (twisting of the tetracene core).

Isostructurality has been analyzed by lattice energy calculations and plots of pairing energy profiles, that reveal at a glance similarities and differences in crystal packing over and above a sometimes dubious comparison of cell parameters. A classic example of isostructurality (and isomorphism) appears for three para-substituted (NO_2 , CF_3 and CN) lateral phenyls, and also surprisingly, a di-thiophene derivative. Three triclinic structures, the parent hydrocarbon, the di-p-nitrophenyl derivative, and a dipyrindine derivative, are also isomorphous. These findings suggest that crystal packing is a driving force that supersedes or at least attenuates the effects of chemical substitution.

Polymorphism is only sparse in the database, the scarce solubility and stability of rubrenes hampering or preventing extensive screenings. Our survey accepts only three cases of undisputable determination: first, the parent hydrocarbon, for which three well determined polymorphs have been deposited, so many presumably because it has been subjected to wider screening efforts; then, the perfluoro compound with two polymorphs, presumably for the same reasons; although our energy calculations strongly suggest that one polymorph is metastable or even unstable.

We report here the structure of a newly found polymorph of the di-p-nitro derivative, obtained after substantial screening: the improved stability toward oxidation of di-p-nitrophenylrubrene allowed crystallization attempts with different solvents affording the monoclinic polymorph or acetone and dichloromethane solvate crystals. The triclinic polymorph has been obtained only by vacuum sublimation with a steeper temperature gradient compared to conditions leading to the monoclinic structure. The comparison of polymorphic energy profiles provides an immediate and univocal proof of the diversity of the crystal packings, the prerequisite for acceptance of a polymorph as a legitimate new material.

A thorough analysis of crystal structures in terms of interaction energies is also fruitful for reliable modeling of crystal morphologies.²⁸ Good agreement between calculated and observed crystal morphologies has been demonstrated for acenes^{40,41} and oligothiophenes.⁴² This approach naturally provides the crystallographic planes and cuts of surfaces reasonably involved in crystal growth processes. Other simpler (and much less demanding) techniques generally provide heavily biased and/or uncomplete results.⁴⁰ The growth morphologies obtained in the present study from analysis of crystal structures via the PBC approach compare satisfactorily with crystals grown from the vapor. The only morphology differing appreciably from the predicted one involves the thienyl derivative. In that case a complex mixture of byproducts (separated with difficulty and incompletely from the main product with column chromatography followed by fractional crystallizations) with molecular structures related to the thienyl rubrene¹⁷ are likely responsible for modification of the crystal morphology.⁵³

The presence of strongly bound (h00) layers in all five analyzed structures arises from the slipped-cofacial arrangement adopted with only small differences. This feature is associated with the strongest periodic bond chains and determines low values for surface energy and attachment energy, respectively determining the equilibrium and growth shape. The similarities in the overall pattern of intermolecular bonds and, hence, of periodic bond chains explain the limited variations of observed growth morphologies. These correspond to crystals defined by Hartman's flat faces characterized by the lowest attachment energies among all possible crystallographic planes. Finally, as already noted in other organic semiconductor crystals, growth morphologies are more anisotropic than equilibrium ones,⁴⁰⁻⁴² with different degrees of tabular shapes where the largest surfaces comprise structural layers based on the slipped-cofacial motif. The corresponding low values for the attachment energy make these crystallographic planes dominate the crystal morphology.

Finally, the insights provided by CLP and PIXEL intermolecular potentials show promise for access to lattice energies and morphology prediction without recourse to computationally intensive quantum chemical methods. As concerns the materials science involved, in general, from our overview it looks like sensitive spots of the driving forces for rubrene packing are the 4-substitution sites at the lateral rings, with substituents of moderate steric bulk. Peripheral substitution at the tetracene core seems to be less influential in steering the packing and hence the physical properties. Our survey provides a structural background that could generate new ideas directing the synthesis of new derivatives and provide hints for the development of enhanced transport properties.

Author Contributions

Massimo Moret (principal investigator) provided the framework for the research project and is mainly responsible for the PBC part. Angelo Gavezzotti developed the methodology for the crystallographic database studies. Both authors concur in the preparation and presentation of the manuscript.

Conflicts of interest

There are no conflicts to declare.

Acknowledgements

Dr. Stefano Bergantin is acknowledged for crystal growth, X-ray data collection and structure refinement of the triclinic polymorph of 5,11-bis(4-nitrophenyl)-6,12-diphenyltetracene.

Notes and references

- J. E. Anthony, *Angew. Chem. Int. Ed.* 2007, **46**, 2-34.
- A. Yassar, *Polym. Sci. Ser. C*, 2014, **56**, 4-19.
- V. Podzorov, V. M. Pudalov and M. E. Gershenson, *Appl. Phys. Lett.* 2003, **82**, 1739-1741.
- V. Podzorov, S. E. Sysoev, E. Loginova, V. M. Pudalov and M. E. Gershenson, *Appl. Phys. Lett.* 2003, **82**, 3504-3506.
- M. L. Clapham, E. C. Murphy and C. J. Douglas, *Synthesis* 2021, **53**, 461-474.
- T. K. Mullenbach, K. A. McGarry, W. A. Luhman, C. J. Douglas and R. J. Holmes, *Adv. Mater.* 2013, **25**, 3689-3693.
- D. A. da Silva Filho, E. G. Kim and J. L. Brédas, *Adv. Mater.* 2005, **17**, 1072-1076.
- M. D. Curtis, J. Cao and J. W. Kampf, *J. Am. Chem. Soc.* 2004, **126**, 4318-4328.
- C. Janiak, *J. Chem. Soc., Dalton Trans.* 2000, 3885-3896.
- V. C. Sundar, J. Zaumseil, V. Podzorov, E. Menard, R. L. Willett, T. Someya, M. E. Gershenson and J. A. Rogers, *Science* 2004, **303**, 1644-1646.
- J. L. Brédas, J. P. Calbert, D. A. da Silva Filho and J. Cornil, *Proc. Nat. Acad. Sci. USA* 2002, **99**, 5804-5809.
- E. Fumagalli, L. Raimondo, L. Silvestri, M. Moret, A. Sassella and M. Campione, *Chem. Mater.* 2011, **23**, 3246-3253.
- S. Bergantin and M. Moret, *Cryst. Growth Des.* 2012, **12**, 6035-6041.
- D. Braga, A. Jaafari, L. Miozzo, M. Moret, S. Rizzato, A. Papagni and A. Yassar, *Eur. J. Org. Chem.* 2011, 4160-4169.
- Y. Sakamoto, T. Suzuki, *J. Org. Chem.* 2017, **82**, 8111-8116.
- K. A. McGarry, W. Xie, C. Sutton, C. Risko, Y. Wu, V. G. Young, J. L. Brédas, C. D. Frisbie and C. J. Douglas, *Chem. Mater.* 2013, **25**, 2254-2263.
- S. Uttiya, L. Miozzo, E. M. Fumagalli, S. Bergantin, R. Ruffo, M. Parravicini, A. Papagni, M. Moret and A. Sassella, *J. Mater. Chem. C* 2014, **2**, 4147-4155.
- C. Sutton, M. S. Marshall, C. D. Sherrill, C. Risko and J. L. Brédas, *J. Am. Chem. Soc.* 2015, **137**, 8775-8782.
- D. Käfer, L. Ruppel, G. Witte and Ch. Wöll, *Phys. Rev. Lett.* 2005, **95**, 166602.
- A. S. Paraskar, A. R. Reddy, A. Patra, Y. H. Wijsboom, O. Gidron, L. J. W. Shimon, G. Leitun and M. Bendikov, *Chem. Eur. J.* 2008, **14**, 10639-10647.
- S. Bergantin, M. Moret, G. Buth and D. P. A. Fabbiani, *J. Phys. Chem. C* 2014, **118**, 13476-13483.
- O. D. Jurchescu, A. Meetsma and T. T. Palstra, *Acta Crystallogr. Sect. B* 2006, **62**, 330-334.

- 1
2
3 23 T. Matsukawa, M. Yoshimura, K. Sasai, M. Uchiyama, M.
4 Yamagishi, Y. Tominari, Y. Takahashi, J. Takeya, Y. Kitaoka, Y.
5 Mori and T. Sasaki, *J. Cryst. Growth* 2010, **312**, 310-313.
6 24 L. Huang, Q. Liao, Q. Shi, H. Fu, J. Ma and J. Yao, *J. Mater.*
7 *Chem.* 2010, **20**, 159-166.
8 25 W. A. Ogden, S. Ghosh, M. J. Bruzek, K. A. McGarry, L. Balhorn,
9 V. Young, L. J. Purvis, S. E. Wegwerth, Z. Zhang, N. A. Serratore,
10 C. J. Cramer, L. Gagliardi and C. J. Douglas, *Cryst. Growth Des.*
11 2017, **17**, 643-658.
12 26 C. Sutton, N. R. Tummala, D. Beljonne and J. L. Brédas, *Chem.*
13 *Mater.* 2017, **29**, 2777-2787.
14 27 M. Mamada, H. Katagiri, T. Sakanoue and S. Tokito, *Cryst.*
15 *Growth Des.* 2015, **15**, 442-448.
16 28 P. Hartman and W. G. Perdok *Acta Crystallogr.* 1955, **8**, 49-52.
17 29 P. Hartman and W. G. Perdok *Acta Crystallogr.* 1955, **8**, 521-
18 524.
19 30 P. Hartman and W. G. Perdok *Acta Crystallogr.* 1955, **8**, 525-
20 529.
21 31 C. R. Groom and F. H. Allen, *Angew. Chem. Int. Ed.* 2014, **53**,
22 662-671.
23 32 A. Gavezzotti, *New J. Chem.* 2011, **35**, 1360-1368.
24 33 A. Gavezzotti, L. Lo Presti and S. Rizzato, *CrystEngComm* 2020,
25 **22**, 7350-7360.
26 34 A. Gavezzotti, *Mol. Phys.* 2008, **106**, 1473-1485 (A. J. Stone
27 Special Issue).
28 35 J. Bernstein, J. D. Dunitz and A. Gavezzotti, *Cryst. Growth Des.*
29 2008, **8**, 2011-2018.
30 36 C. Greenwell and G. J. O. Beran, *J. Mater. Chem. C* 2021, **9**,
31 2848-2857.
32 37 P. Hartman, *Morphology of Crystals*, (Ed.: I. Sunagawa), Terra
33 Scientific Publishing Company, Tokyo, 1997, pp. 269-319.
34 38 P. Hartman and P. Bennema, *J. Cryst. Growth* 1980, **49**, 145-
35 156.
36 39 P. Hartman and H-K. Chan, *Pharm. Res.* 1993, **10**, 1052-1058.
37 40 F. R. Massaro, M. Moret, M. Bruno, M. Rubbo and D. Aquilano,
38 *Cryst. Growth Des.* 2011, **11**, 4639-4646.
39 41 F. R. Massaro, M. Moret, M. Bruno and D. Aquilano, *Cryst.*
40 *Growth Des.* 2012, **12**, 982-989.
41 42 F. R. Massaro, M. Moret, M. Bruno and D. Aquilano, *Cryst.*
42 *Growth Des.* 2013, **13**, 1334-1341.
43 43 C. F. R. A. C. Lima, J. C. S. Costa, L. M. S. S. Lima, A. Melo, A. N.
44 M. S. Silva and L. M. N. B. F. Santos, *ChemistrySelect* 2017, **2**,
45 1759-1769.
46 44 H. Morisaki, T. Koretsune, C. Hotta, J. Takeya, T. Kimura and Y.
47 Wakabayashi, *Nat. Comm.* 2014, **5**, 5400.
48 45 R. Kern, *Morphology of Crystals*, (Ed.: I. Sunagawa), Terra
49 Scientific Publishing Company, Tokyo, 1997, pp. 77-206.
50 46 B. D. Chapman, A. Checco, R. Pindak, T. Siegrist and C. Kloc, *J.*
51 *Cryst. Growth* 2006, **290**, 479-484.
52 47 T. Minato, H. Aoki, H. Fukidome, T. Wagner and K. Itaya, *Appl.*
53 *Phys. Lett.* 2009, **95**, 093302.
54 48 M. El Helou, O. Medenbach and G. Witte, *Cryst. Growth Des.*
55 2010, **10**, 3496-3501.
56 49 D. Käfer and G. Witte, *Phys. Chem. Chem. Phys.* 2007, **7**, 2850-
57 2853.
58 50 S. Bergantin, Organic semiconductor rubrene: crystal
59 chemistry of derivatives and high-pressure polymorphism,
60 PhD Thesis in Materials Science, Università di Milano-Bicocca,
2014.
51 T. Matsukawa, Y. Takahashi, T. Tokiyama, K. Sasai, Y. Murai, N.
52 Hirota, Y. Tominari, N. Mino, M. Yoshimura, M. Abe, J. Takeya,
53 Y. Kitaoka, Y. Mori, S. Morita and T. Sasaki, *Jap. J. Appl. Phys.*
54 2008, **47**, 8950-8954.
55 L. Carman, H. P. Martinez, L. Voss, S. Hunter, P. Beck, N.
56 Zaitseva, S. A. Payne, P. Irkhin, H. H. Choi and V. Pozdorov, *IEEE*
57 *Trans. Nucl. Sci.* 2017, **64**, 781-788.
58 53 K. Sangwal, *Additives and crystallization processes*, John Wiley
59 and Sons, Chichester, 2007.

1
2
3 Electronic Supplementary Information (ESI) for New Journal of Chemistry
4
5
6
7

8 **The crystalline state of rubrene materials: intermolecular recognition,**
9 **isomorphism, polymorphism, and periodic bond-chain analysis of**
10 **morphologies**
11
12
13
14

15 Massimo Moret,^a and Angelo Gavezzotti^b
16
17
18

19 ^aDepartment of Materials Science, University of Milano - Bicocca (Italy)
20
21

22 E-mail massimo.moret@unimib.it
23

24 ^bDepartment of Chemistry, University of Milano (retired) (Italy)
25
26

27 E-mail angelo.gavezzotti@unimi.it
28
29
30
31
32
33
34
35
36
37
38
39
40
41
42
43
44
45
46
47
48
49
50
51
52
53
54
55
56
57
58
59
60

Appendix: crystallographic terminology

Throughout the article, the following notations/terms are extensively used:

[uvw] crystallographic direction. Any direction in a Bravais lattice is identified by a set of N indices (N dimensionality of the space), written in square brackets, called the direction indices. In three-dimensional space, the direction passing through the origin and the lattice nodes nu, nv, nw (n integer) has direction indices $[uvw]$. The indices $[-u, -v, -w]$ identify the same direction as $[uvw]$ observed from the opposite side.

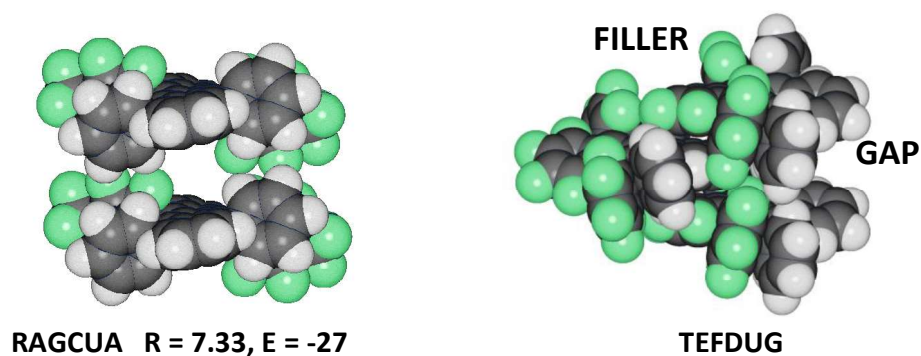
<uvw> set of symmetry related crystallographic directions according to space group symmetry

(hkl) crystallographic plane identified by its Miller indices

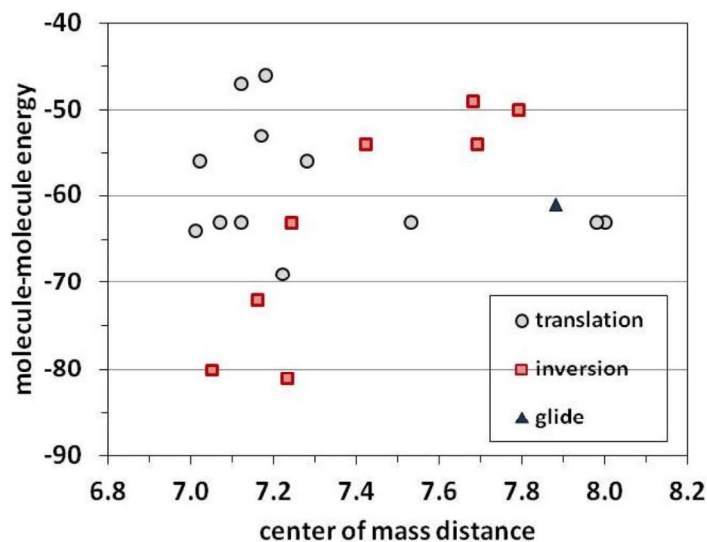
{hkl} set of symmetry related crystallographic planes (form) according to space group symmetry

isomorphous crystals: two crystals are said to be isomorphous if (a) both have the same space group and unit-cell dimensions and (b) the types and the positions of atoms in both are the same except for a replacement of one or more atoms in one structure with different types of atoms in the other (diadochy), such as heavy atoms, or the presence of one or more additional atoms in one of them (*isomorphous addition*). Isomorphous crystals can form *solid solutions*

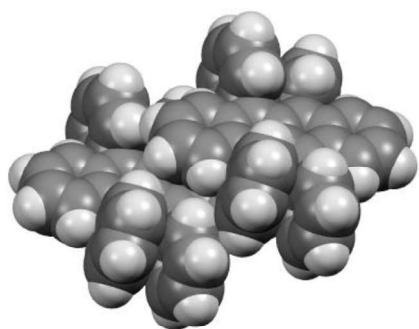
isostructural crystals: Two crystals are said to be *isostructural* if they have the same structure, but not necessarily the same cell dimensions nor the same chemical composition, and with a 'comparable' variability in the atomic coordinates to that of the cell dimensions and chemical composition. One also speaks of *isostructural series*. The term isotopic is synonymous with isostructural.



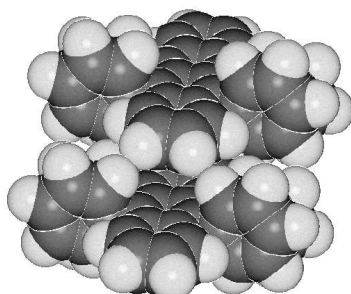
15 **Figure S1.** RAGCUA, short distance coupling with low stabilization due to parallel tetracene cores without offset.
 16 TEFDUG, close packing is restored by the insertion of another filler in the gap. These structures are outliers in the top
 17 left part of Figure 2b. Fluorine is green.



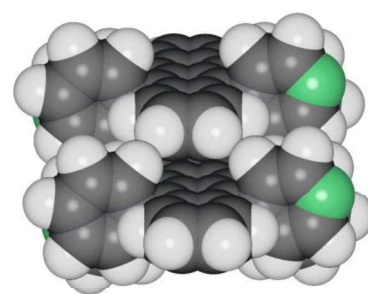
39 **Figure S2.** Molecule-Molecule energy (kJ/mol) vs. center of mass distance for the subset of slipped-cofacial pairings
 40 out of Figure 2b. No correlation



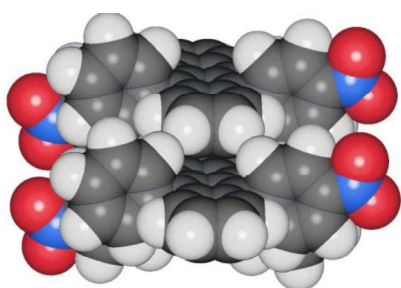
QQCIG05



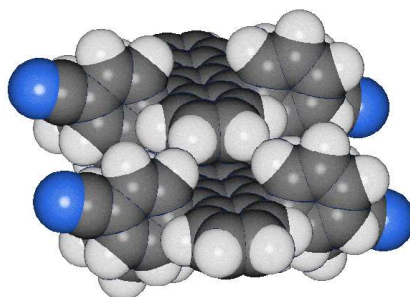
QQCIG14



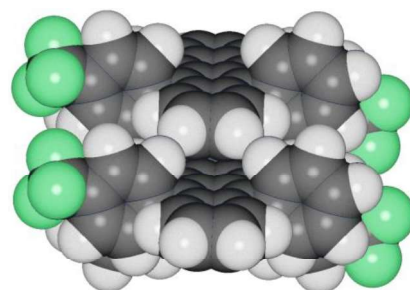
VICHAT



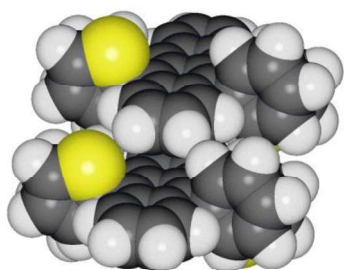
CIYNAB



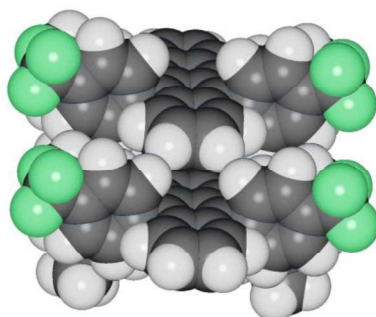
CIYXUF



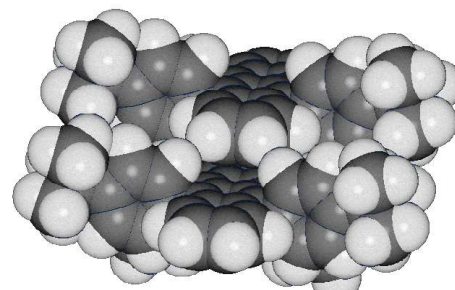
CIYYAM



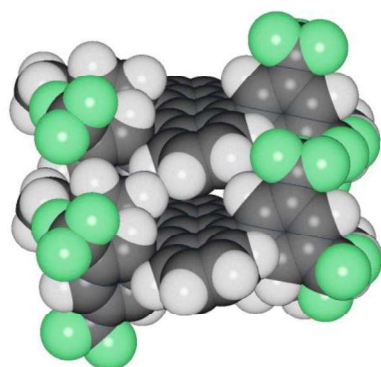
PIXPUJ



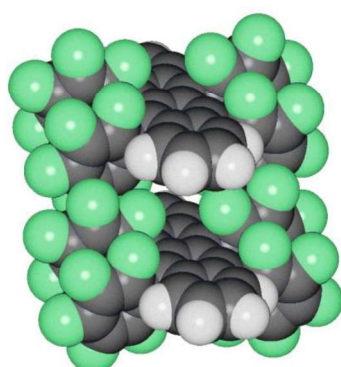
MIVDOM



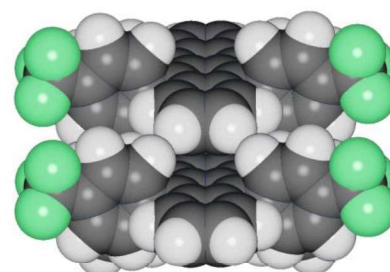
PIFHIW



RAGCEK



RAGDIP



MIVDUS

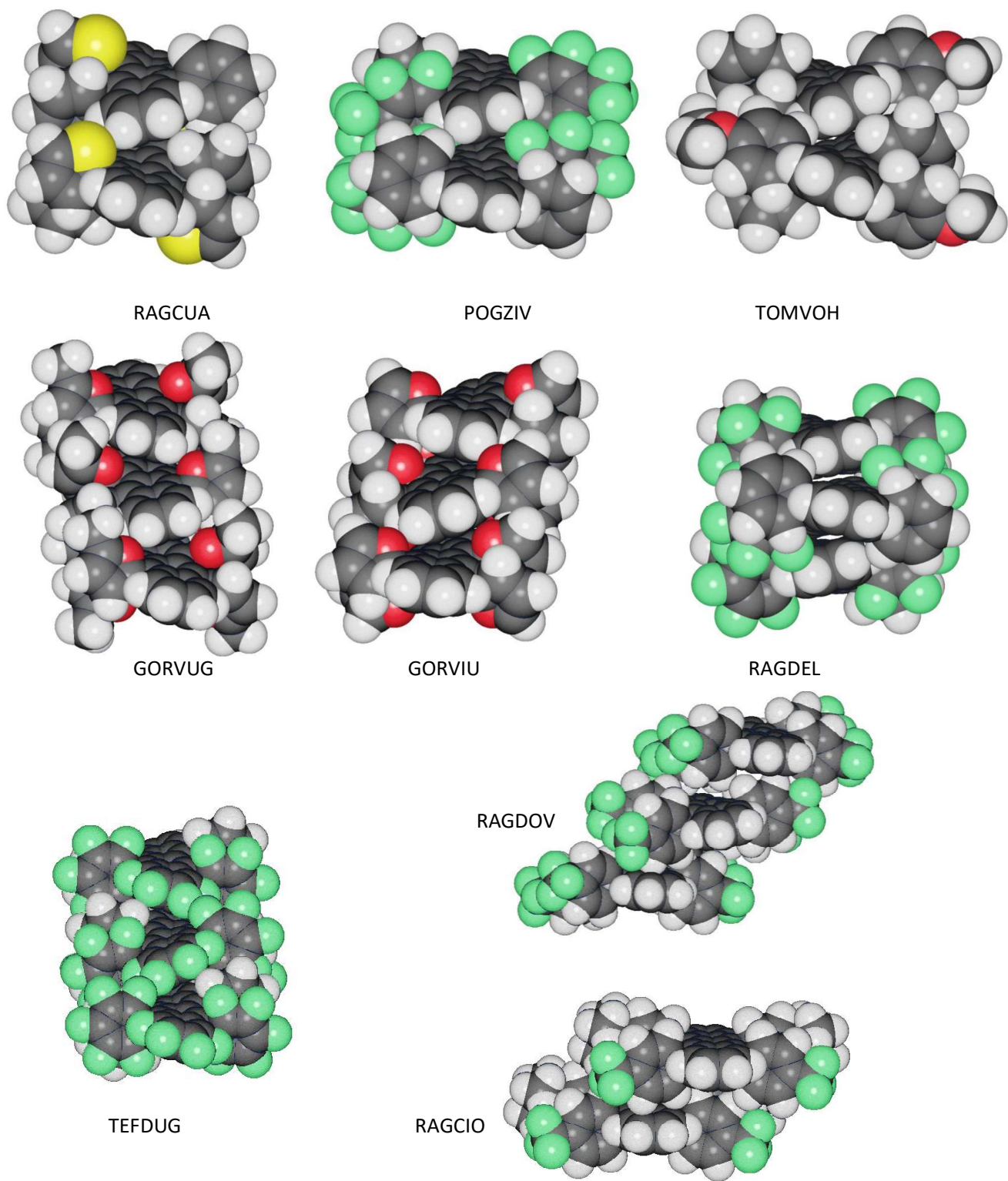


Figure S3. A gallery of slipped-cofacial arrangements with CSD refcodes (see Table 1).

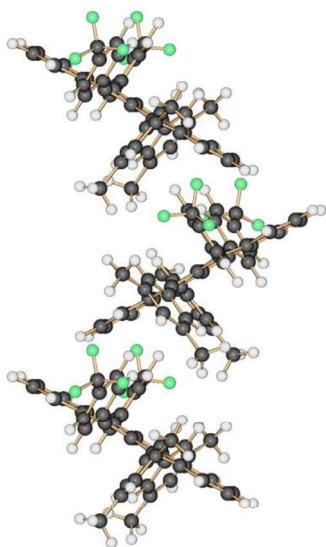


Figure S4. MIVDOM: the screw axis sequence $-x, y \pm 1/2, 3/2-z$ with a very stabilizing pairwise energy; $R(\text{mm})=7.91 \text{ \AA}$, $E(\text{mm})=-70 \text{ kJ mol}^{-1}$.

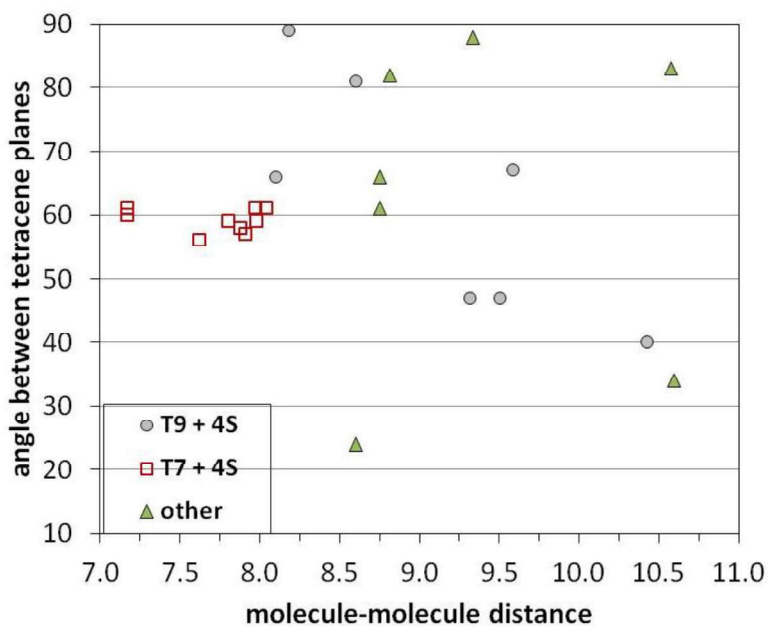
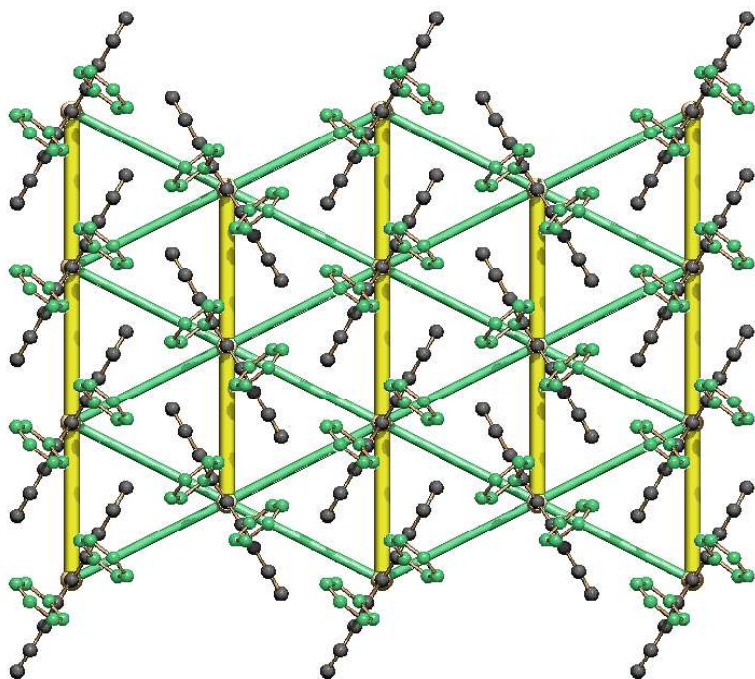
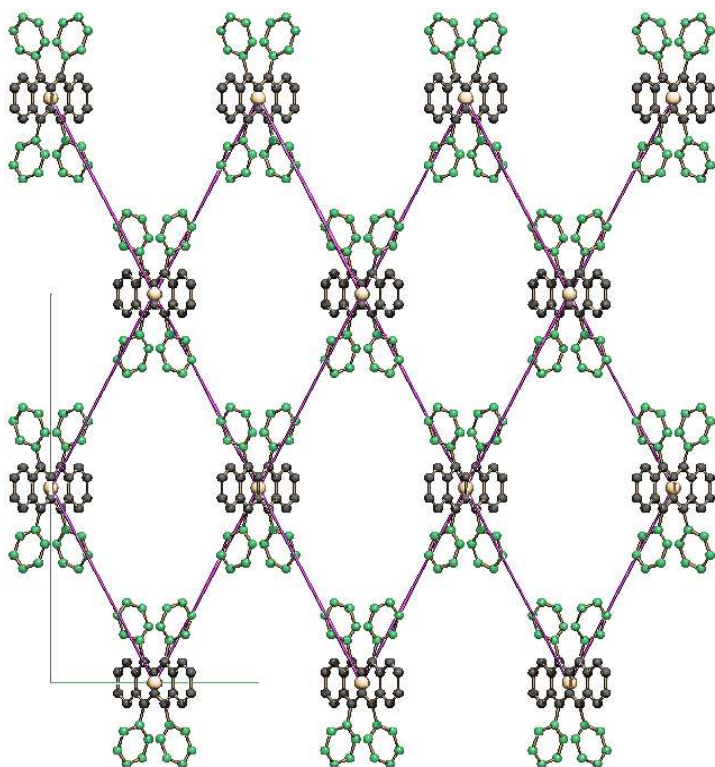


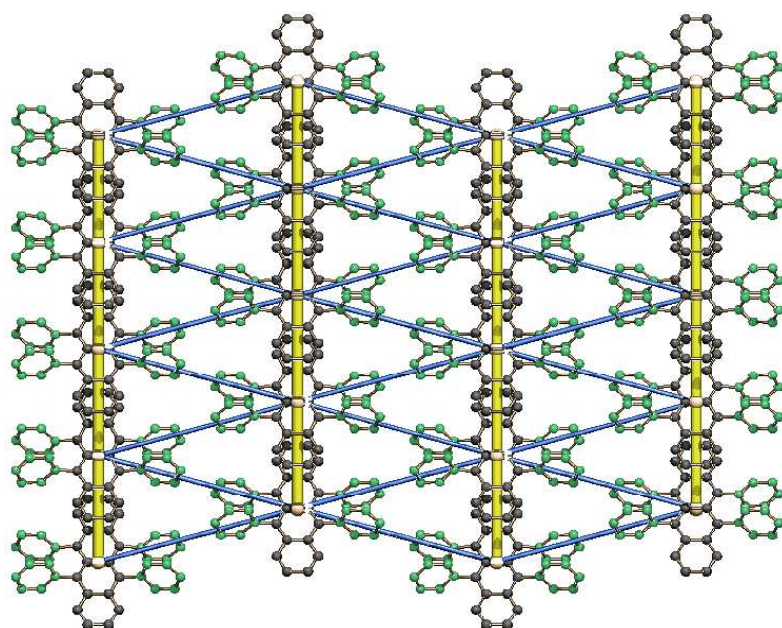
Figure S5. Plot of angles between tetracene planes in corrugated (herringbone) propagation motifs. The T7+4S cage motif (Figure 6a) has consistently a 60° angle.



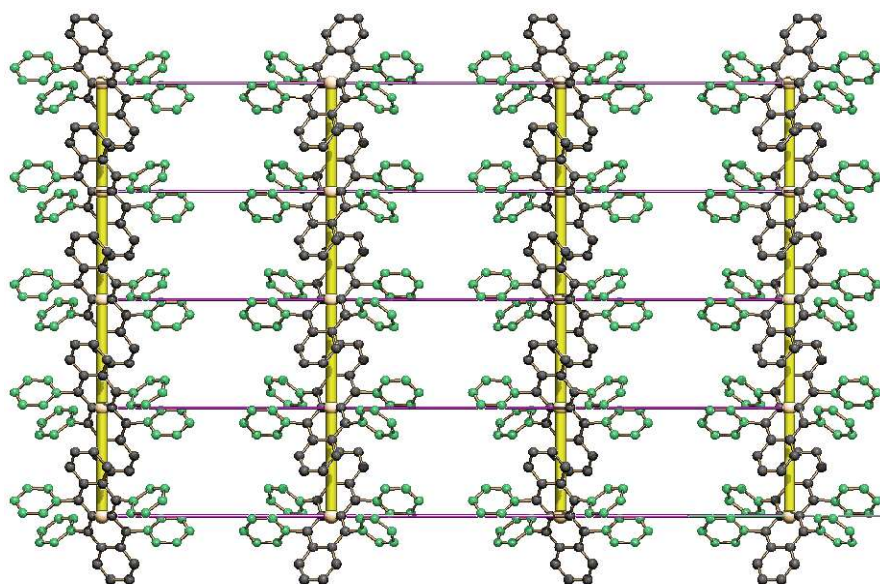
slice (200)



slice (020)



slice (002)



slice (202)

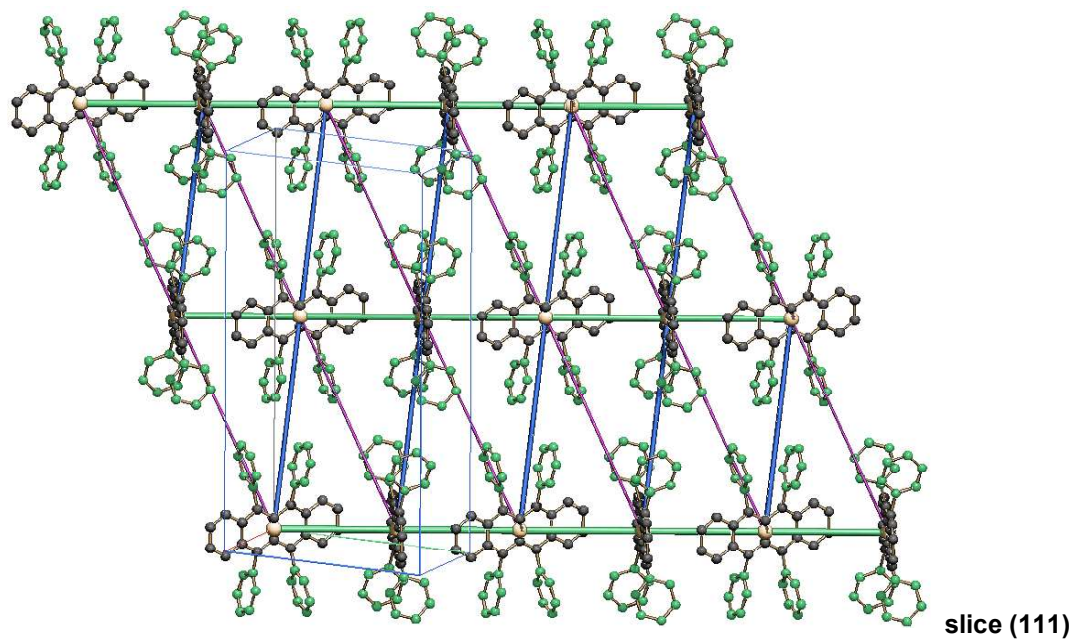
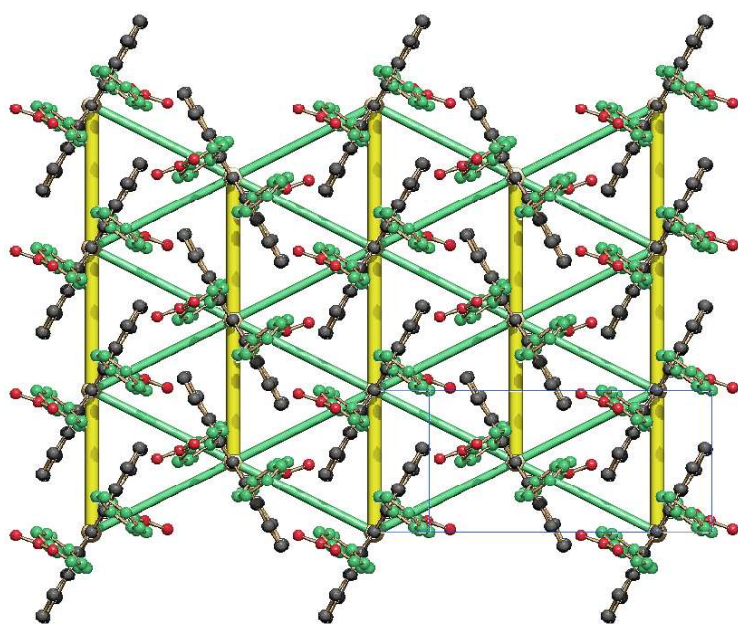
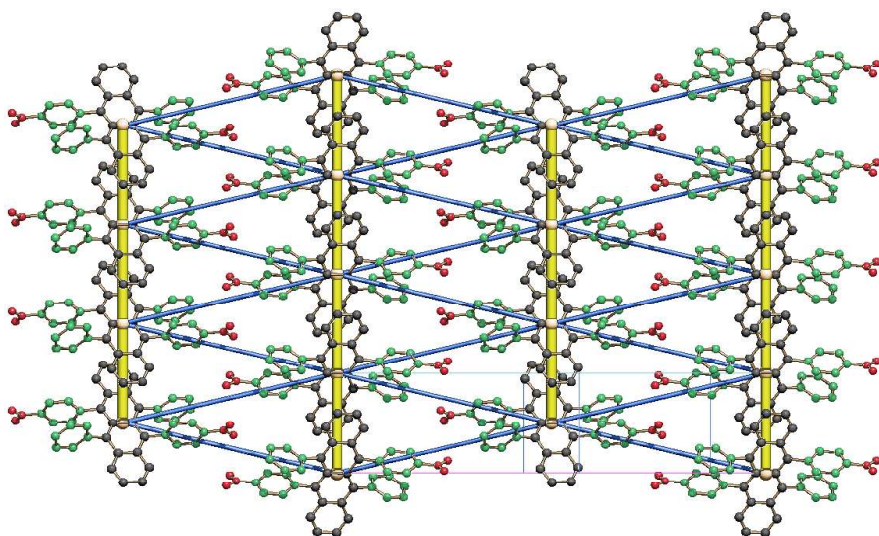


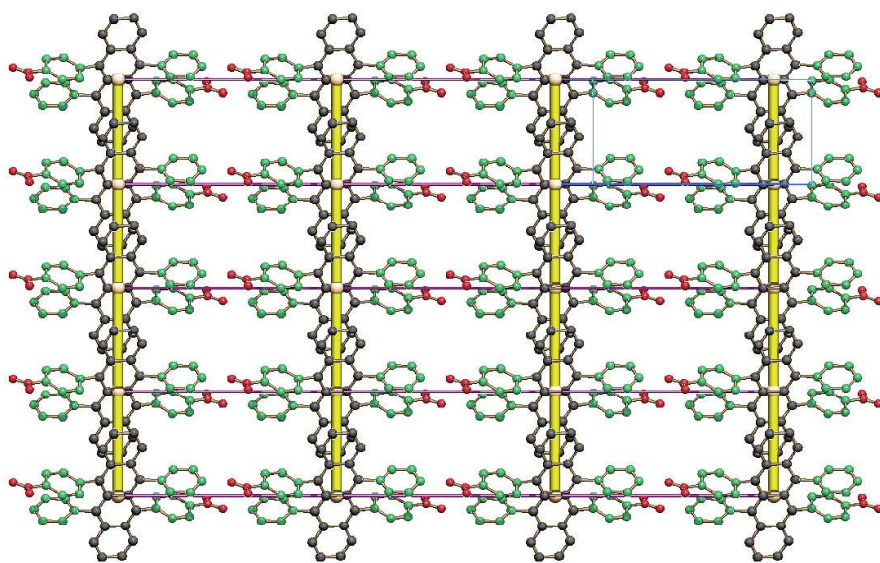
Figure S6. Energy crystal graphs in rubrene (QQCIG05). Intermolecular bonds (see Table 3 in the manuscript) are color coded as: bond **a** yellow, bond **b** green, bond **c** cyan, bond **c** purple. All molecular plots and crystal graphs were prepared with program SCHAKAL (E. Keller SCHAKAL99, University of Freiburg - Germany, 1999).



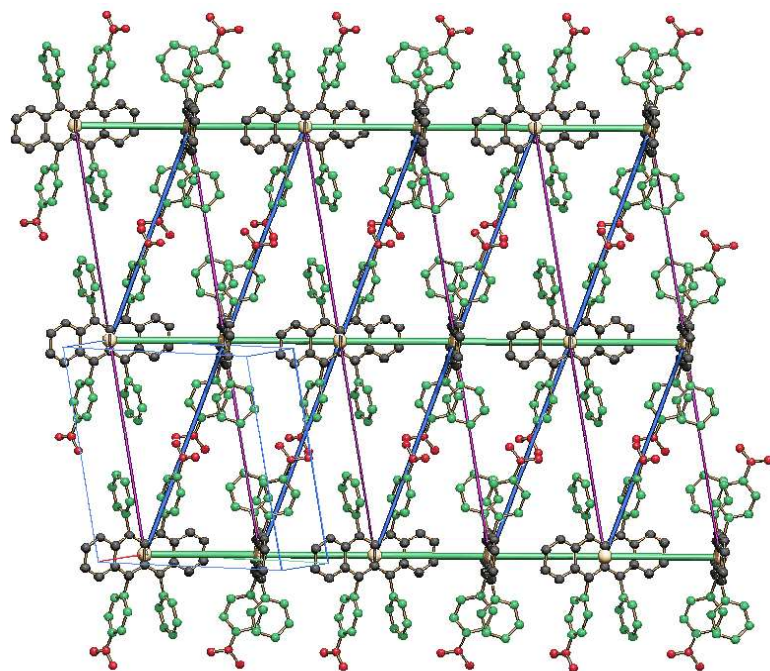
slice (100)



slice (10-2)



slice (002)



slice (011)

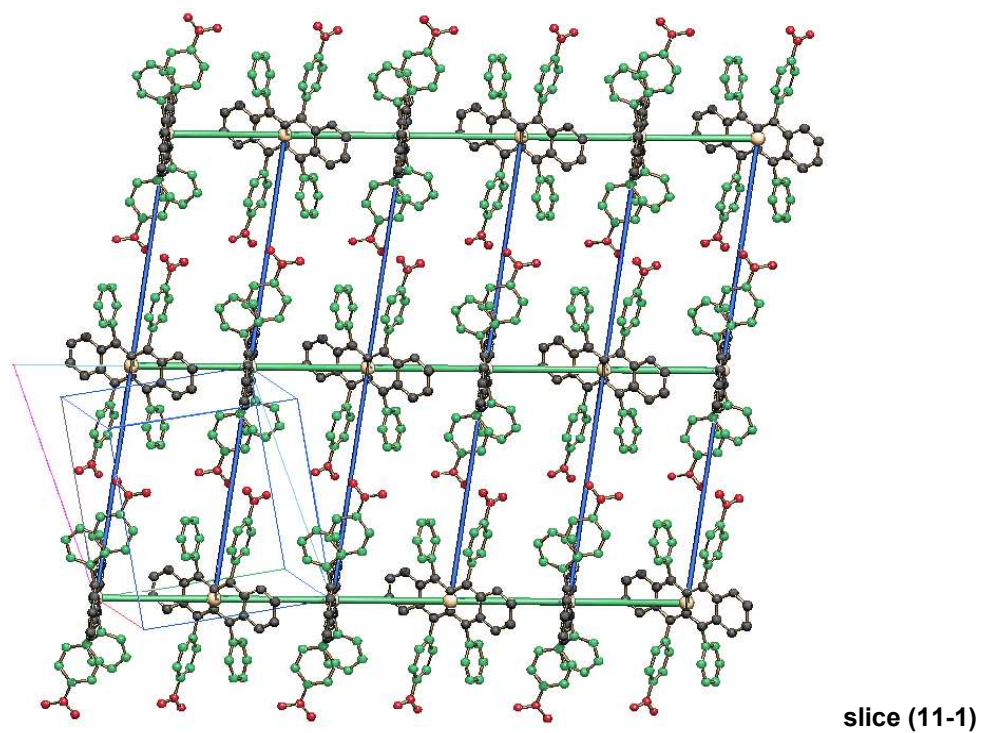


Figure S7. Energy crystal graphs in 5,11-bis(4-nitrophenyl)-6,12-diphenyltetracene (CIYNAB). Intermolecular bonds (see Table 4 in the manuscript) are color coded as: bond **a** yellow, bond **b** green, bond **c** cyan, bond **c** purple.

TABLE S1. List of all the rubrene crystal structures in the Cambridge Structural Database. From left to right: Identification code of the Cambridge Structural Database (CSD), Crystallographic *R*-factor, Spce group, Molecules in unit cell, Molecules in asymmetric unit, Temperature of data collection (K), Cell parameters (Å and degrees), Unit cell volume (Å³), Reduced cell parameters (Å and degrees), Reduced cell volume (Å³).

Refcode	Rfac	Space Group	Z	Z'	T	a	b	c	α	β	γ	Volume	Reduced a	Reduced b	Reduced c	Reduced α	Reduced β	Reduced γ	Reduced Volume
AXIDER	6.35	P21/c	2	0.5	293	9.0298	9.909	16.217	90	90.227	90	1451	9.0298	9.9085	16.217	90	90.227	90	1451
CIYNAB	6.73	P21/c	2	0.5	153	15.098	7.171	14.249	90	100.616	90	1516.2	7.1706	14.2489	15.0983	100.616	90	90	1516
CIYXUF	6.59	P21/c	2	0.5	123	15.978	7.276	13.981	90	102.701	90	1585.7	7.2762	13.9814	15.9782	102.701	90	90	1586
CIYYAM	6.65	P21/c	2	0.5	120	14.913	7.115	14.426	90	98.099	90	1515.4	7.1151	14.4263	14.9125	98.099	90	90	1515
GORVEQ	7.77	P212121	4	1	93	9.599	13.29	25.015	90	90	90	3190.5	9.599	13.287	25.015	90	90	90	3190
GORVIU	4.59	P-1	3	1.5	93	10.553	11.34	16.568	83.481	89.45	64.275	1772.9	10.553	11.34	16.568	83.481	89.45	64.275	1773
GORVIU01	4.6	P21/c	4	1	93	14.386	8.452	21.794	90	116.994	90	2361.2	8.452	14.386	19.9328	103.0291	90	90	2361
GORVUG	4.5	P-1	2	1	93	8.5037	13.24	14.277	62.458	80.781	74.581	1373.1	8.5037	13.244	14.277	62.458	80.781	74.581	1373
INELUK	5.62	P21/n	4	1	123	16.665	11.15	19.192	90	90.213	90	3565.8	11.1489	16.6651	19.1918	90.213	90	90	3566
INELUK01	6.87	P-1	6	3	123	12.529	17.82	24.734	90.202	101.264	90.695	5414	12.5285	17.8163	24.7339	90.202	101.264	90.695	5414
INELUK02	4.5	P21/c	2	0.5	173	8.9017	10.53	17.992	90	90.408	90	1686	8.9017	10.527	17.992	90	90.408	90	1686
INELUK03	7.34	P21/n	4	1	173	16.635	11.13	19.245	90	90.581	90	3564.1	11.1334	16.635	19.245	90.581	90	90	3564
KUSDEJ	5.27	Cmca	4	0.25	173	34.197	7.158	14.052	90	90	90	3439.5	7.1577	14.052	17.469	90	101.8218	90	1720
MIVCUR	4.75	C2/c	12	1.5	173	41.257	10.15	24.038	90	96.739	90	9993	10.1464	21.2432	24.038	96.5431	90	103.8166	4997
MIVDAY	4.31	P21	2	1	173	12.75	9.414	14.503	90	99.576	90	1716.4	9.4141	12.7495	14.5027	99.576	90	90	1716
MIVDEC	4.21	Pna21	4	1	173	15.205	13.9	14.31	90	90	90	3024.6	13.901	14.3104	15.2045	90	90	90	3025
MIVDIG	9.52	Pbcm	4	0.5	123	7.1443	14.05	34.143	90	90	90	3427.4	7.1443	14.051	34.143	90	90	90	3427
MIVDOM	7.61	Pbcm	4	0.5	123	7.5317	14.63	32.424	90	90	90	3573.7	7.5317	14.634	32.424	90	90	90	3574
MIVDUS	4.59	Pnma	4	0.5	123	7.1162	31.18	14.208	90	90	90	3152.3	7.1162	14.2075	31.179	90	90	90	3152
PIFHIW	7.42	Pnma	4	0.5	292	14.158	35.39	7.2215	90	90	90	3618.3	7.2215	14.158	35.39	90	90	90	3618
PIFHOC	9.77	P21/c	4	1	292	23.527	9.028	17.764	90	95.928	90	3752.8	9.0277	17.764	23.527	95.928	90	90	3753
PIXPOD	4.3	P21	2	1	173	11.401	8.994	13.989	90	113.59	90	1314.6	8.9944	11.401	13.989	113.59	90	90	1315
PIXPOD01	5.01	P21/c	4	1	93	13.601	9.248	20.718	90	92.771	90	2602.9	9.2479	13.601	20.718	92.771	90	90	2603
PIXPUJ	6.49	P21/c	2	0.5	173	10.173	8.915	14.751	90	95.17	90	1332.3	8.9148	10.173	14.751	95.17	90	90	1332
PIXPUJ01	6.87	P21/c	2	0.5	120	13.568	7.014	14.302	90	103.954	90	1320.9	7.0143	13.5679	14.302	103.954	90	90	1321
POGZIV	6.91	P21/c	8	2	294	22.036	8.803	30.252	90	104.921	90	5670.8	8.8034	22.036	30.252	104.921	90	90	5671

Refcode	Rfac	Space Group	Z	Z'	T	a	b	c	α	β	γ	Volume	Reduced a	Reduced b	Reduced c	Reduced α	Reduced β	Reduced γ	Reduced Volume
QQQCIG		Aba2	4	0.5	295	14.44	7.18	26.97	90	90	90	2796.2	7.18	13.9547	14.44	90	90	104.908	1398
QQQCIG01	3.2	Bbam	4	0.25	295	7.184	14.43	26.897	90	90	90	2788.9	7.184	13.9199	14.433	90	90	104.954	1394
QQQCIG02			1	0	295	9.15	11.6	7.16	103.53	112.97	90.98	675.28	0	0	0	0	0	0	0
QQQCIG03		P21/a	2	0.5	295	15.5	10.1	8.8	90	90.55	90	1377.6	8.8	10.1	15.5	90	90.55	90	1378
QQQCIG04	3.72	Cmca	4	0.25	100	26.789	7.17	14.211	90	90	90	2729.6	7.17	13.866	14.211	90	90	104.984	1365
QQQCIG05	3.77	Cmca	4	0.25	125	26.789	7.173	14.246	90	90	90	2737.5	7.173	13.8664	14.246	90	90	104.990	1369
QQQCIG06	3.87	Cmca	4	0.25	150	26.775	7.168	14.258	90	90	90	2736.4	7.168	13.8589	14.258	90	90	104.987	1368
QQQCIG07	3.88	Cmca	4	0.25	175	26.828	7.181	14.306	90	90	90	2756.1	7.181	13.8862	14.306	90	90	104.985	1378
QQQCIG08	4.07	Cmca	4	0.25	200	26.838	7.181	14.332	90	90	90	2762.1	7.181	13.8911	14.332	90	90	104.980	1381
QQQCIG09	4.05	Cmca	4	0.25	235	26.818	7.174	14.348	90	90	90	2760.4	7.174	13.8805	14.348	90	90	104.976	1380
QQQCIG10	4.19	Cmca	4	0.25	275	26.938	7.211	14.461	90	90	90	2809	7.211	13.9432	14.461	90	90	104.986	1405
QQQCIG11	4.4	Cmca	4	0.25	293	26.86	7.193	14.433	90	90	90	2788.5	7.193	13.9032	14.433	90	90	104.992	1394
QQQCIG12		Cmca	4	0.25	295	26.901	7.187	14.43	90	90	90	2789.9	7.187	13.9223	14.43	90	90	104.958	1395
QQQCIG13	4.94	P21/c	2	0.5	173	8.7397	10.13	15.635	90	90.98	90	1383.3	8.7397	10.125	15.635	90	90.98	90	1383
QQQCIG14	6.72	P-1	1	0.5	173	7.0196	8.543	11.948	93.04	105.58	96.28	683.5	7.0196	8.5432	11.948	93.04	105.58	96.28	684
QQQCIG15	4.02	Bbcm	4	0.25	293	7.175	14.44	26.812	90	90	90	2776.9	7.175	13.8777	14.435	90	90	104.981	1388
QQQCIG16	4.6	Cmca	4	0.25	100	26.797	7.162	14.194	90	90	90	2724	7.1617	13.8689	14.194	90	90	104.963	1362
QQQCIG17	2.2	Cmca	4	0.25	100	26.811	7.16	14.203	90	90	90	2726.5	7.1602	13.8751	14.2029	90	90	104.953	1363
QQQCIG18	2.2	Cmca	4	0.25	100	26.811	7.16	14.203	90	90	90	2726.5	7.1602	13.8751	14.2029	90	90	104.953	1363
QQQCIG19	4.7	Cmca	4	0.25	100	26.811	7.16	14.203	90	90	90	2726.5	7.1602	13.8751	14.2029	90	90	104.953	1363
QQQCIG20	3.3	Cmca	4	0.25	100	26.811	7.16	14.203	90	90	90	2726.5	7.1602	13.8751	14.2029	90	90	104.953	1363
QQQCIG21	2.57	Cmca	4	0.25	100	26.811	7.16	14.203	90	90	90	2726.5	7.1602	13.8751	14.2029	90	90	104.953	1363
QQQCIG22	2.2	Cmca	4	0.25	100	26.811	7.16	14.203	90	90	90	2726.5	7.1602	13.8751	14.2029	90	90	104.953	1363
QQQCIG23	2	Cmca	4	0.25	20	26.797	7.16	14.152	90	90	90	2715.2	7.1599	13.8683	14.1519	90	90	104.960	1358
QQQCIG24	5.89	P-1	1	0.5	293	7.0478	8.55	11.949	93.201	105.501	96.079	687.21	7.0478	8.5495	11.9485	93.201	105.501	96.079	687
QQQCIG25	4.5	P-1	1	0.5	293	6.8535	8.264	11.657	91.614	104.921	96.311	633.03	6.8535	8.2642	11.6573	91.614	104.921	96.311	633
QQQCIG26	6.02	P-1	1	0.5	293	6.7392	8.059	11.464	90.271	104.627	96.329	598.44	6.7392	8.0591	11.4641	90.271	104.627	96.329	598
QQQCIG27	6.56	P-1	1	0.5	293	6.6779	7.926	11.342	89.367	104.46	96.321	577.63	6.6779	7.9256	11.3415	89.367	75.54	83.679	578
QQQCIG28	6.39	P-1	1	0.5	293	6.635	7.8	11.218	88.437	104.348	96.316	559.02	6.635	7.7995	11.2182	88.437	75.652	83.684	559
QQQCIG29	5.61	P-1	1	0.5	293	6.6162	7.676	11.1	87.399	104.322	96.289	542.81	6.6162	7.6757	11.1002	87.399	75.678	83.711	543
QQQCIG30	6	P-1	2	1	293	14.24	6.774	11.281	81.264	100.378	101.773	1040.3	6.7738	11.281	14.2395	79.622	78.227	81.264	1040

Refcode	Rfac	Space Group	Z	Z'	T	a	b	c	α	β	γ	Volume	Reduced a	Reduced b	Reduced c	Reduced α	Reduced β	Reduced γ	Reduced Volume
QQQCIG31	5.24	P-1	1	0.5	293	7.0883	8.599	12.006	93.486	105.642	95.977	697.86	7.0883	8.5994	12.0059	93.486	105.642	95.977	698
QQQCIG32	5.26	P-1	1	0.5	293	7.082	8.58	11.982	93.36	105.63	96.02	694.41	7.082	8.58	11.982	93.36	105.63	96.02	694
QQQCIG33	2.56	Cmca	4	0.25	100	26.797	7.162	14.194	90	90	90	2724	7.1617	13.8689	14.194	90	90	104.963	1362
RAGCEK	5.59	P21/c	4	1	123	15.88	29.54	7.9956	90	91.745	90	3749.2	7.9956	15.88	29.5419	90	90	91.745	3749
RAGCIO	6.14	P2/c	4	1	123	31.29	7.403	17.207	90	90.524	90	3985.7	7.403	17.2071	31.2902	90.524	90	90	3986
RAGCOU	6.82	P21	4	2	123	16.408	15.28	16.446	90	97.838	90	4084	15.2768	16.4083	16.4464	97.838	90	90	4084
RAGCUA	3.74	C2/c	4	0.5	123	31.027	14.68	7.3302	90	93.322	90	3332.5	7.3302	14.6772	17.1618	115.316	93.003	90	1666
RAGDAH	3.23	P21/n	4	1	123	14.856	9.198	27.452	90	103.528	90	3647.1	9.1983	14.8556	27.4515	103.528	90	90	3647
RAGDEL	4.71	P-1	2	1	123	7.3564	14.7	15.712	65.973	88.823	89.903	1551.9	7.3564	14.7042	15.7118	65.973	88.823	89.903	1552
RAGDIP	3.89	P-1	2	1	123	7.9792	12.79	16.774	92.313	95.376	105.306	1640.5	7.9792	12.793	16.7743	92.313	95.376	105.306	1641
RAGDOV	7.13	C2/c	4	0.5	123	18.275	16.4	14.486	90	126.468	90	3490.8	12.2764	12.2764	14.2549	110.888	114.307	96.201	1745
TEFDUG	7.48	Pnna	4	0.5	173	15.521	28.08	7.3931	90	90	90	3222.2	7.3931	15.5207	28.081	90	90	90	3222
TOMVOH	4.15	Pbca	8	1	120	15.766	13.86	28.351	90	90	90	6194.7	13.859	15.766	28.351	90	90	90	6195
TOMVUN	5.49	Cmca	4	0.25	120	27.45	7.102	14.327	90	90	90	2793	7.102	14.1769	14.327	90	90	104.506	1397
TOMWAU	5.59	P21/n	4	1	120	17.677	9.424	18.571	90	103.79	90	3004.5	9.424	17.677	18.571	103.79	90	90	3005
VICHAT	4.09	P-1	1	0.5	100	7.0727	8.27	11.855	90.402	106.039	97.605	659.84	7.0727	8.2696	11.855	90.402	106.039	97.605	660

Table S2. Comparison of the CLP, LJC and Pixel force fields for some molecule-molecule energies in some isostructural rubrene derivatives. For each entry:

molecule-molecule distance (Å), symmetry operation number
 LJC energies (kJ mol⁻¹), Coulombic, polarization, dispersion, repulsion, total
 PIXEL energies, id.
 CLP energies, id.

	symmetry operation		cell translation			
	1	x, y, z				
	2	-x, 1/2+y, 1/2-z	screw axis			
CIYXUF	7.880	2	0.00	-0.50	-0.50	
	-6.7	0.0	-73.9	27.4		-53.2
	-17.21	-7.26	-64.40	38.08		-50.79
	-6.1	-4.7	-58.8	18.6		-51.0
	7.276	1	0.00	-1.00	0.00	
	8.2	0.0	-109.9	41.4		-60.4
CIYYAM	-3.88	-10.47	-97.94	54.91		-57.38
	7.7	-5.2	-87.9	29.7		-55.7
	8.043	2	0.00	-0.50	-0.50	
	-5.3	0.0	-62.9	20.7		-47.4
	-13.28	-5.98	-57.73	29.46		-47.53
	-4.6	-4.0	-50.6	12.8		-46.4
CIYNAB	7.115	1	0.00	-1.00	0.00	
	11.7	0.0	-107.8	39.6		-56.5
	-1.09	-11.51	-97.73	54.06		-56.26
	10.5	-5.0	-87.1	34.5		-47.2
	7.976	2	0.00	-0.50	-0.50	
	-5.5	0.0	-70.2	24.7		-51.0
CIYXUF	-14.71	-7.28	-62.94	34.60		-50.34
	-4.1	-4.9	-56.0	15.6		-49.4
	7.171	1	0.00	-1.00	0.00	
	11.6	0.0	-109.7	42.4		-55.6
	-1.84	-12.79	-99.26	57.06		-56.84
	11.2	-5.5	-88.5	36.7		-46.0

Table S3. Energy (CLP) and density data for the crystal structures in the database.

For each entry:

first line: CSD refcode Cell vol (Å³) density (g cm⁻³) packing factorsecond line: CSD refcode Ecoul Epol Edisp Erep Etot (kJ mol⁻¹)

AXIDER	P21/c	1450.95	1.384	0.721		
AXIDER	P21/c	-11.8	-26.2	-228.3	69.7	-196.6
CIYNAB	P21/c	1516.24	1.364	0.738		
CIYNAB	P21/c	-19.3	-35.1	-269.3	107.8	-215.8
CIYNAB01	P-1	775.14	1.334	0.718		
CIYNAB01	P-1	-15.0	-32.1	-243.0	73.2	-216.8
CIYXUF	P21/c	1585.71	1.401	0.716		
CIYXUF	P21/c	-7.5	-29.1	-256.7	86.9	-206.5
CIYYAM	P21/c	1515.42	1.277	0.723		
CIYYAM	P21/c	-24.8	-29.5	-251.7	83.9	-222.1
GORVIU01	P21/c	2361.24	1.386	0.736		
GORVIU01	P21/c	-17.1	-26.9	-230.3	77.0	-197.2
GORVUG	P-1	1373.07	1.327	0.724		
GORVUG	P-1	-11.7	-49.5	-259.8	100.0	-221.0
INELUK	P21/n	3565.76	1.931	0.723		
INELUK	P21/n	-34.6	-35.4	-229.3	115.1	-184.2
INELUK02	P21/c	1685.96	2.042	0.765		
INELUK02	P21/c	-47.5	-38.6	-262.4	133.4	-215.1
MIVCUR	C2/c	9993.03	1.174	0.680		
MIVCUR	C2/c	-8.3	-29.7	-231.0	75.0	-194.0
MIVDOM	Pbcm	3573.74	1.347	0.704		
MIVDOM	Pbcm	-7.2	-40.5	-257.9	81.7	-223.9
PIFHOC	P21/c	3752.80	1.141	0.672		
PIFHOC	P21/c	-5.8	-35.7	-226.6	59.6	-208.5
PIXPOD01	P21/c	2602.88	1.421	0.724		
PIXPOD01	P21/c	-16.4	-40.5	-241.7	72.0	-226.6
PIXPUJ01	P21/c	1320.94	1.370	0.740		
PIXPUJ01	P21/c	-8.3	-31.2	-250.3	68.2	-221.5
POGZIV	P21/c	5670.76	1.276	0.685		
POGZIV	P21/c	-2.4	-27.7	-206.6	53.0	-183.7
RAGDAH	P21/n	3647.07	1.531	0.700		
RAGDAH	P21/n	-19.4	-37.8	-241.9	105.8	-193.2
MIVDAY	P21	1716.43	1.194	0.699		
MIVDAY	P21	-9.5	-36.4	-250.3	76.8	-219.4
MIVDEC	Pna21	3024.61	1.231	0.709		
MIVDEC	Pna21	-7.0	-26.3	-241.6	76.2	-198.7
MIVDUS	Pnma	3152.30	1.409	0.719		
MIVDUS	Pnma	-4.0	-29.1	-252.5	82.4	-203.2
PIFHIW	Pnma	3618.34	1.184	0.697		
PIFHIW	Pnma	-2.5	-37.5	-262.0	65.2	-236.9
QQQCIG05	Cmca	2737.48	1.293	0.739		
QQQCIG05	Cmca	-9.8	-22.7	-252.0	79.3	-205.1
QQQCIG13	P21/c	1383.33	1.279	0.731		
QQQCIG13	P21/c	-15.7	-22.3	-241.6	72.7	-206.8
QQQCIG14	P-1	683.50	1.294	0.740		
QQQCIG14	P-1	-4.1	-22.8	-246.4	76.9	-196.4
RAGCEK	P21/c	3749.20	1.475	0.703		

RAGCEK	P21/c	-7.1	-40.9	-252.8	97.1	-203.7
RAGCIO	P2/c	3985.71	1.301	0.696		
RAGCIO	P2/c	-9.8	-45.6	-257.1	79.7	-232.7
RAGCUA	C2/c	3332.51	1.620	0.728		
RAGCUA	C2/c	-10.4	-34.2	-254.3	113.7	-185.3
RAGDEL	P-1	1551.92	1.525	0.715		
RAGDEL	P-1	-13.8	-25.8	-230.4	105.8	-164.1
RAGDIP	P-1	1640.50	1.807	0.737		
RAGDIP	P-1	-17.0	-32.3	-245.1	108.4	-186.0
RAGDOV	C2/c	3490.80	1.531	0.718		
RAGDOV	C2/c	-17.8	-37.1	-262.9	96.2	-221.6
TEFDUG	Pnna	3222.18	1.617	0.714		
TEFDUG	Pnna	-26.6	-28.0	-231.8	108.1	-178.3
TOMVOH	Pbca	6194.72	1.271	0.718		
TOMVOH	Pbca	-10.7	-30.0	-256.7	86.8	-210.7
TOMWAU	P21/n	3004.53	1.324	0.720		
TOMWAU	P21/n	-19.5	-28.0	-250.4	98.3	-199.5
VICHAT	P-1	659.84	1.346	0.755		
VICHAT	P-1	-13.1	-24.3	-263.2	85.6	-215.0

Table S4. A summary of pairwise molecular couplings with the slipped cofacial configuration. Distances in Å, energies (AA-CLP) in kJ mol⁻¹. T, translation, Inv inversion, other operations with coordinate transformation.

translation				
CIYNAB	7.171	-46	Ty	
CIYXUF	7.276	-56	Ty	
CIYYAM	7.115	-47	Ty	
PIXPUJ	7.014	-64	Ty	
PIFHIW	7.221	-69	Tz	
MIVDOM	7.532	-63	Tx	
QQQCIG05	7.173	-53	Ty	
QQQCIG14	7.020	-56	Tx	
RAGCEK	7.996	-63	Tz	
RAGDIP	7.979	-63	Tx	
VICHAT	7.073	-63	Tx	
MIVDUS	7.116	-63	Tx	
other				
RAGCUA	7.418	-54	Inv	1 0 0
POGZIV	7.687	-54	Inv	0 1 2
TOMVOH	7.884	-61	x,y,-z	½, 0, ½
RAGDEL	7.676	-49	Inv	1 0 1
	7.791	-50	Inv	0 0 1
GORVIU	7.157	-72	Inv	1 0 0
	7.241	-63	Inv	2 0 0
GORVUG	7.051	-80	Inv	1 0 1
	7.231	-81	Inv	1 0 2
offset				
RAGCIO	7.403	-71	Ty	
RAGDOV	7.538	-77	Inv	0 1 1
	7.538	-77	Inv	0 1 2

Table S5. Extended motifs in the packing of rubrenes. Contacts with highest molecule-molecule contact energies.

Codes: SC7 (O): slipped cofacial at 7 Å distance; Operator = T, I, S

T7 = ≈ 7 Å translation, T9 = ≈ 9 Å translation; I = inversion, T = translation, S = screw, G = glide

4S: four identical screw operations, 2S: two screw related molecules

refcode Z SC motif

P-1 space groups

CIYNAB01	1	SC7(T)	
GORVUG	2	SC7(I)	
QQQCIG14	1	SC7(T)	
RAGDEL	2	SC7(I)	
VICHAT	1	SC7(T)	

C2/c space group Z'=1/2

RAGCUA	4	SC7(T)	
RAGDOV	4	SC7(I)	

Others

GORVIU01	4	SC7(I)	P21/c
TOMVOH	8	SC7(S)	Pbca
CIYNAB	2	SC7(T) T7+4S	P21/c
CIYXUF	2	SC7(T) T7+4S	P21/c
CIYYAM	2	SC7(T) T7+4S	P21/c
PIXPUJ01	2	SC7(T) T7+4S	P21/c
PIFHIW	4	SC7(T) T7+4S	Pnma
QQQCIG05	4	SC7(T) T7+4S	Cmca
MIVDOM	4	SC7(T) T7+2S+2S	Pbcm
MIVDUS	4	SC7(T) T7+2S+2S	Pnma

Other fourfold cage coordinations (no SC)

AXIDER	2	T9+4S	P21/c
INELUK02	2	T9+4S	P21/c
QQQCIG13	2	T9+4S	P21/c
PIXPOD01	4	T9+2S+2S	P21/c
MIVDAY	2	T9+2S+2S	P21
RAGDAH	4	T9+2S+2S	P21/n
PIFHOC	4	T9+2G+2G	P21/c

Approximate or no classification

INELUK	4	2I+2S+2T	P21/n
MIVDEC	4	mix G, S	Pna21
RAGCEK	4	mix T, I, G	P21/c
RAGCIO	4	T7+4G (no SC)	P2/c
TEFDUG	4	T7+4G (no SC)	Pnna
TOMWAU	4	mix T, I, S, G	P21/n

Z' > 1: MIVCUR, POGZIV, RAGDIP not analyzed

Table S6. Surface energies (erg cm⁻²) for selected isomorphous monoclinic rubrenes.

	CIYNAB	CIYXUF	CIYYAM	PIXPUJ01
Form	Surface energy			
{100}	102.5	54.5	105.2	86.4
{10 $\bar{2}$ }	86.1	78.5	86.3	89.9
{011}	107.8	89.0	103.3	88.4
{002}	86.3	79.4	85.3	92.8
{11 $\bar{1}$ }	93.7	80.6	90.5	103.0